Steady-state water exchange in neural tissue is primarily passive and through the phospholipid bilayer

Nathan H. Williamson[1,2,3,4 *], **Rea Ravin**[1,5 *], **Teddy X. Cai**[1], **Julian A. Rey**[1,6], **and Peter J. Basser**[1] ✉

[1] *Eunice Kennedy Shriver* National Institute of Child Health and Human Development, National Institutes of Health, Bethesda, MD 20892, USA
[2] Military Traumatic Brain Injury Initiative (MTBI[2]), Bethesda, Maryland 20814, USA
[3] Uniformed Services University of the Health Sciences (USU), Bethesda, Maryland 20814, USA
[4] The Henry M. Jackson Foundation for the Advancement of Military Medicine, Inc. (HJF), Bethesda, Maryland 20817, USA
[5] Celoptics, Rockville, MD 20850, USA
[6] National Institute of General Medical Sciences, National Institutes of Health, Bethesda, MD 20892, USA
[*] N.H.W. and R.R. contributed equally to this work.

Correspondence: ***basserp@mail.nih.gov***
This article was deposited on BioRxiv as a preprint `https://doi.org/10.1101/2024.12.12.628254`

Classification: Biological Sciences – Physiology
Keywords: homeostasis, diffusion exchange spectroscopy (DEXSY), tissue microstructure, porous media, membrane permeability, low-field single-sided NMR, apparent diffusion coefficient (ADC), gray matter

ABSTRACT

Water molecules exchange incessantly across cell membranes and between intracellular compartments, but the dominant steady-state transport pathways——and whether they are active or passive——remain unclear. Low-field, high-gradient diffusion exchange spectroscopy (DEXSY) nuclear magnetic resonance (NMR) measurements on viable *ex vivo* neonatal mouse spinal cords show that water exchange is primarily passive. The apparent exchange rate constant (AXR) depends on osmotic conditions because it reflects multiple exchange pathways, each weighted by the exchanging compartments' volume fractions. A faster transmembrane path which becomes more visible with increasing extracellular fraction has a high activation energy but is ion-independent, suggesting passive transport through the phospholipid bilayer and not transport through co-transporter or channel proteins. A slower pathway which dominates when the extracelluar space is shrunken has a low activation energy, consistent with geometric exchange between intracellular environments. Moreover, we show how DEXSY can be used to non-invasively measure tonicity in tissue, and inform us about the status of the tissue millieu. These findings may also inform future translation to clinical MRI.

SIGNIFICANCE STATEMENT

Despite water's abundance and essential role in life, few techniques allow direct interrogation of steady-state water transport and homeostasis at the cellular level in tissue. We demonstrate that diffusion exchange spectroscopy (DEXSY) NMR fills this gap by addressing two fundamental questions: How does water exchange between tissue microenvironments under steady-state conditions, and do these processes involve active water cycling? A key result is a method to non-invasively estimate tonicity in tissue.

Introduction

Water is the solvent of life, yet details of its movement across cell membranes remains an enigma. Water molecules continuously exchange between intracellular and extracellular spaces under steady-state conditions without net flow or cell volume changes. However, the dominant transmembrane transport pathways——and whether they involve energetically-active mechanisms or only thermally-driven passive diffusion——are not fully understood.[1] Noninvasive MRI techniques can image water exchange,[2–5] but unlocking their full diagnostic potential requires a deeper understanding of the mechanism.

Among techniques for probing water exchange, diffusion-based NMR methods[6] are emerging as the most translatable to *in vivo* MRI of the CNS, compared with contrast agent–based approaches.[7] By encoding water displacements with magnetic field gradients, apparent diffusion coefficients (ADC) provide indirect measures of cellular microstructure. With two gradient encodings separated by a mixing time, diffusion exchange spectroscopy (DEXSY) reveals water movement between compartments with distinct ADC values.[8,9] Stronger gradients access diffusion and exchange on smaller length scales and faster timescales.[10–12] With gradients tuned appropriately, water restricted inside the cell has a much lower ADC than water outside, and ADC is inversely related to cell volume.[13] With ADC contrast between inside and outside, the apparent exchange rate constant (AXR) is sensitive to transmembrane exchange[14] and, without other contributions, is proportional to the membrane surface-to-volume ratio SVR and diffusive permeability to water.[15,16]

Passive water exchange involves water diffusing through the membrane lipid bilayer or channels, driven only by thermal motion.[17] Sensitivity of exchange to active ion transport inhibitors led to the "active water cycling" (AWC) hypothesis in which water moves in tandem with ions through transporters.[18–20] Unlike contrast agent-based methods, diffusion-based methods can be additionally sensitive to diffusion-mediated, geometric exchange between compartments with differing sizes and orientations relative to the gradient direction.[21] While these suggest AXR can be a biomarker for both metabolism and microstructure, the factors governing AXR in geometrically-complex, metabolically-active tissues remain unclear.[21–23]

Active, passive, and geometric exchange mechanisms potentially intersect in CNS gray matter. CNS is the most metabolically active organ per unit mass, with roughly half of that energy being devoted to active ion transport by the Na^+/K^+–ATPase.[24] Active water cycling (AWC) in gray matter was inferred from contrast-agent studies showing that ouabain inhibition of the Na^+/K^+–ATPase strongly reduces water exchange.[19] This was later supported by low-field, high-gradient DEXSY measurements showing a 70% reduction in AXR.[12] Studies of isolated lipid components suggest that passive membrane permeability could be high[25,26] and, coupled with the the high SVR,[27,28] could account for fast AXR. Geometric exchange between cell soma and branching processes can also be significant.[28] Simultaneous transmembrane and geometric exchange produces multi-site exchange, introducing cell volume dependencies which simulations showed could account for the 70% AXR reduction.[29] Importantly, active ion transport maintains cell volume,[30] making it difficult to disentangle its alleged direct effect on transmembrane water exchange from an indirect effect on AXR via changes in cell volume. To resolve this, it is necessary to control for tonicity, allowing perturbation of active ion transport independent of cell volume.

Tonicity is defined by the osmolarity of intracellular and extracellular solutes, taking their permeability into account. This inherently affects extracellular space (ECS) and intracellular space (ICS) volume fractions. Intracellular impermeants (metabolites, proteins, nucleic acids, etc.) and positively charged counterions that accompany them due to their net-negative fixed charge create a persistent osmotic load.[30,31] This load is normally balanced by ions partitioned through active and downstream passive transport processes. In animal cells, the Na^+/K^+–ATPase is the primary active transporter. When the Na^+/K^+–ATPase is inhibited, the balance is lost and extracellular hypotonicity causes cells to swell. However, in *ex vivo* experiments, osmolytes such as sucrose or mannitol can be added to the bathing media to control extracellular tonicity.[27] While tonicity is a critical determinant of water homeostasis, it is difficult or (previously) impossible to measure non-invasively.

In this low-field, high-gradient DEXSY NMR study of viable *ex vivo* spinal cord, we isolate the effects of active ion transport inhibition from those of tonicity changes. Our results indicate that transmembrane water exchange in this system does not involve significant active water cycling (AWC). Instead, changes in AXR following Na^+/K^+–ATPase inhibition arise from altered tonicity. The data are consistent with passive multi-site exchange, with fast transmembrane exchange between ECS and ICS, and slower geometric exchange between ICS compartments. Under isotonic and hypertonic conditions (i.e., shrunken cells), AXR is fast and exhibits a high activation energy, consistent with passive transmembrane exchange through the phospholipid bilayer. In contrast, hypotonic conditions (i.e., swollen cells) yield slower AXR with a lower activation energy, suggesting water movement through aqueous pathways such as geometric exchange between intracellular regions. In this multi-site exchange mechanism, the intrinsic permeability of each pathway remains constant, but the measurement sensitivity shifts with tonicity through changes in ECS volume fraction. Together with other diffusion metrics, AXR may provide a quantitative biomarker of cellular function, with implications for assessing tissue health and pathology.

Results

Active ion transport inhibition has a large effect on AXR and simultaneously a smaller effect on ADC. AXR and ADC_y were collected during perturbations with 2, 10, and 100 μM ouabain. Here, the subscript "y" refers to the gradient (and hence diffusion encoding) direction, which is perpendicular to the orientation of the spinal cord. 100 μM ouabain is expected to maximally inhibit the Na^+/K^+–ATPase, while 2 and 10 μM ouabain are expected to result in partial inhibition.[32] Effects are compared to baseline recordings. Samples maintain stable AXR and ADC_y for many hours under normal conditions (Figs. 1G, S2D, and Ref. 12) and have been found to be electrically-active afterwards.[11] In this system we find that ADC acts as a proxy for diffusion and DEXSY-derived volume fractions, as seen by their strong linear correlation (see Supplement and Figs. S1 and S5). This is expected, due to the high gradient strength defining a sensitivity to restriction length scales of roughly 1 micron[11,33], well-tuned to the length scales of cell processes which occupy the majority of the tissue[28]. Volume fractions were also estimated, but are presented only as supplemental material to reduce redundancy.

Ouabain simultaneously decreased ADC_y and AXR (Fig. 1 and Fig. S2). ADC_y and AXR were affected precipitously, within 11 minutes after the addition of 100 μM ouabain (Fig. 1A,D,G,H). At 10 μM ouabain, the effect was delayed but still precipitous (Fig. 1G,H). At 2 μM ouabain, the effect was delayed further but occurred on average within 150 min of addition (Fig. 1B,E,G,H). The effect of 2 μM was precipitous in some cases (Fig. 1B,E) but less so overall (Fig. 1G). Subsequent exposure to higher ouabain concentrations did not produce any further effect (Fig. 1B,E). Nevertheless, the impact of the initial dose of ouabain on ADC_y was influenced by the concentration (Fig. 1C). 2, 10 and 100 μM ouabain decreased ADC_y by $5.6 \pm 3.1\%$, $8.6 \pm 1.8\%$, and $10.5 \pm 2.2\%$, respectively (significantly different between groups, $p < 0.001$, see Fig. 1C). In comparison, AXR was much more affected by ouabain, but it depended less on the dosage. AXR is $131 \pm 19\ s^{-1}$ under normal conditions. Ouabain reduced AXR by $72 \pm 7\%$ (averaged across the three concentration groups, Fig. 1F). 2 μM ouabain reduced AXR to $43.8 \pm 6.8\ s^{-1}$ (significantly different from the other concentration groups, $p < 0.001$). 10 and 100 μM ouabain reduced AXR to 35.2 ± 6.0 and $35.6 \pm 8.2\ s^{-1}$, respectively (not significantly different, $p = 0.857$). The similar precipitous but delayed effect across dosages (with only a small difference at the lowest 2 μM concentration) is reminiscent of an "all-or-none" effect. The coincident effect on ADC_y suggests that cells swelled when the drop in AXR occurred. Simulations also predict that deactivating the Na^+/K^+–ATPase causes

cell swelling and membrane depolarization due to the redistribution of ions (Fig. S3).[29]

We tested whether there was a correlation between AXR and ADC_y. First, the relative change from baseline of $\Delta\mathrm{ADC}_y$ and Δk are plotted for all measurements in the ouabain treated groups (Fig. 1F inset). The correlation is significant but weak (correlation coefficient $cc = 0.45$, $p < 0.001$) and is insignificant when the 2 μM data is omitted ($p = 0.7$). A linear fit of the data yields $\Delta k = 1.05 \times \Delta\mathrm{ADC}_y - 63.0\ \%$. Note that the y-intercept is shifted well below 0. This will be explained in the discussion. Next, the data is grouped based on whether ouabain was administered and correlations between the absolute values of ADC_y and AXR are presented. The two groups do not share the same correlation (Fig. 1I). ADC_y and AXR showed a weak positive correlation under normal conditions ($cc = 0.20$, $p = 0.01$) and a weak negative correlation after ouabain took effect ($cc = -0.21$, $p = 0.03$). Note that the correlation seen when plotting ADC_y as a percent change from baseline appears much different than when plotting the absolute value (compare Fig. 1F inset to Fig. 1I). This is due to differences between samples which are accounted for when normalizing to the baseline (compare Fig. 1C to Fig. S2C). Although AXR and ADC_y are both affected by ouabain, they measure different tissue properties.

These results are consistent with previous studies,[12,19] and could be construed as evidence for AWC. However, it is difficult to completely rule out the possibility that these results could be explained by more complicated microstructural effects since active ion transport and cell volume are normally interlinked and are both affected by $\mathrm{Na}^+/\mathrm{K}^+$–ATPase inhibition.

AXR is not directly linked to ion transport, voltage, or active water cycling. Certain cotransporters have been shown to cotransport water with ions.[34–38] Similarly, the AWC mechanism, which involves water actively cycling along with ions through the $\mathrm{Na}^+/\mathrm{K}^+$–ATPase and other downstream transporters, was proposed to explain the effect of ouabain on AXR.[19,20] Here we further test this AWC hypothesis by studying the effects of $\mathrm{Na}^+/\mathrm{K}^+$–ATPase inhibition independent from volume changes. Since the $\mathrm{Na}^+/\mathrm{K}^+$–ATPase pumps ions to control tonicity and cell volume under normal conditions,[30] we used an osmolyte to compensate for tonicity changes induced by $\mathrm{Na}^+/\mathrm{K}^+$–ATPase inhibition. Specifically, we used an aCSF media in which the major ionic component, 128.35 mM NaCl, was replaced with 256.7 mM sucrose (Fig. 2A,B). This was inspired by electrophysiology studies that use 0 NaCl, high sucrose media to maintain viability of adult animal brain slices.[39] Compared to normal aCSF, the 0 NaCl, 256.7 mM sucrose media has an equal osmolarity but a higher tonicity because membranes are impermeable to sucrose but are semipermeable to Na^+ and Cl^- (Fig. S3). Note that the media still has 21.58 mM Na^+ and 7 mM Cl^- from salts other than NaCl.

The 0 NaCl, 256.7 mM sucrose media caused $\Delta\mathrm{ADC}_y$ to increase significantly ($p < 0.001$), by $2.1 \pm 1.3\%$, because its higher tonicity shrunk cells slightly (Fig. 2A,E). If water actively cycles along with ions, then the transmembrane exchange rate constant would decrease when washing to 0 NaCl, 256.7 mM sucrose media because $\mathrm{Na}^+/\mathrm{K}^+$–ATPase activity is reduced and any potential AWC membrane influx proteins acting as Na^+ and Cl^- cotransporters should be reduced considerably. Instead, AXR increased significantly ($p < 0.001$), by $27 \pm 24\%$, and 10 μM ouabain had no additional effect ($p = 0.7$) (Fig. 2A,F). When ouabain was added first and was present through the whole experiment, the 0 NaCl, 256.7 mM sucrose media subsequently raised AXR significantly above normal levels ($p < 0.001$) (Fig. 2B,F). Therefore, AXR is not directly linked to $\mathrm{Na}^+/\mathrm{K}^+$–ATPase activity, but instead to the tonicity that the $\mathrm{Na}^+/\mathrm{K}^+$–ATPase establishes.

In order to distinguish effects related to voltage from effects related to cell volume, normal aCSF media was washed to media in which the 128.35 mM NaCl was replaced with 128.35 mM sodium gluconate. Gluconate is a monovalent anion and does not pass through the plasma membrane.[40] Due to electroneutrality, for every anion of gluconate in the ECS there will also be a cation (ignoring divalent cations). Therefore, 128.35 mM sodium gluconate adds 256.7 mOsm of osmotic pressure. The resulting pressure is the same as replacing 128.35 mM NaCl with 256.7 mM sucrose. Thus these medias are expected to have the same effect on tonicity, but the $\mathrm{Na}^+/\mathrm{K}^+$–ATPase can still be active in the sodium gluconate media since Na^+ is still present in high concentration. Simulations predict that cells can maintain voltage polarization with this media, but unlike in normal media, they depolarize *without* a change in volume when the $\mathrm{Na}^+/\mathrm{K}^+$–ATPase is inactivated (Fig. S3).[29] This is because gluconate does not flow into the cell following the loss of membrane potential as chloride would.

We found that washing to sodium gluconate media had no significant effect on $\mathrm{ADC_y}$ or AXR ($p = 0.9$ and $p = 0.6$, respectively) (Fig. 2C,E,F). Adding 10 μM ouabain on top of sodium gluconate media caused $\mathrm{ADC_y}$ to increase significantly ($p = 0.02$), indicating cellular shrinkage. AXR also increased significantly ($p < 0.001$), in the opposite direction of what the AWC hypothesis would predict. Note these results are unlike what was observed above, where washing to 0 NaCl, 256.7 mM sucrose media had an effect but then adding ouabain had no further effect. Interestingly, AXR values under sodium gluconate + 10 μM ouabain conditions were similar to those obtained under 0 NaCl, 256.7 mM sucrose media conditions (2-sample t-test, $p = 0.001$). Given their different ionic strengths but similar tonicity, this suggests AXR is related to volumetric conditions or tonicity but is not directly linked to ion transport, voltage, or AWC.

The lack of effect when washing to sodium gluconate followed by the effect when adding ouabain could be evidence of cell volume regulation.[41] The data variability increased after ouabain addition, which could be due to slow changes occurring during the measurement and the system not being at a true steady-state. Experiments were repeated with ouabain being added before washing to sodium gluconate media and yielded consistent results (Fig. 2D,E,F).

We conclude from the results above that steady-state trans-

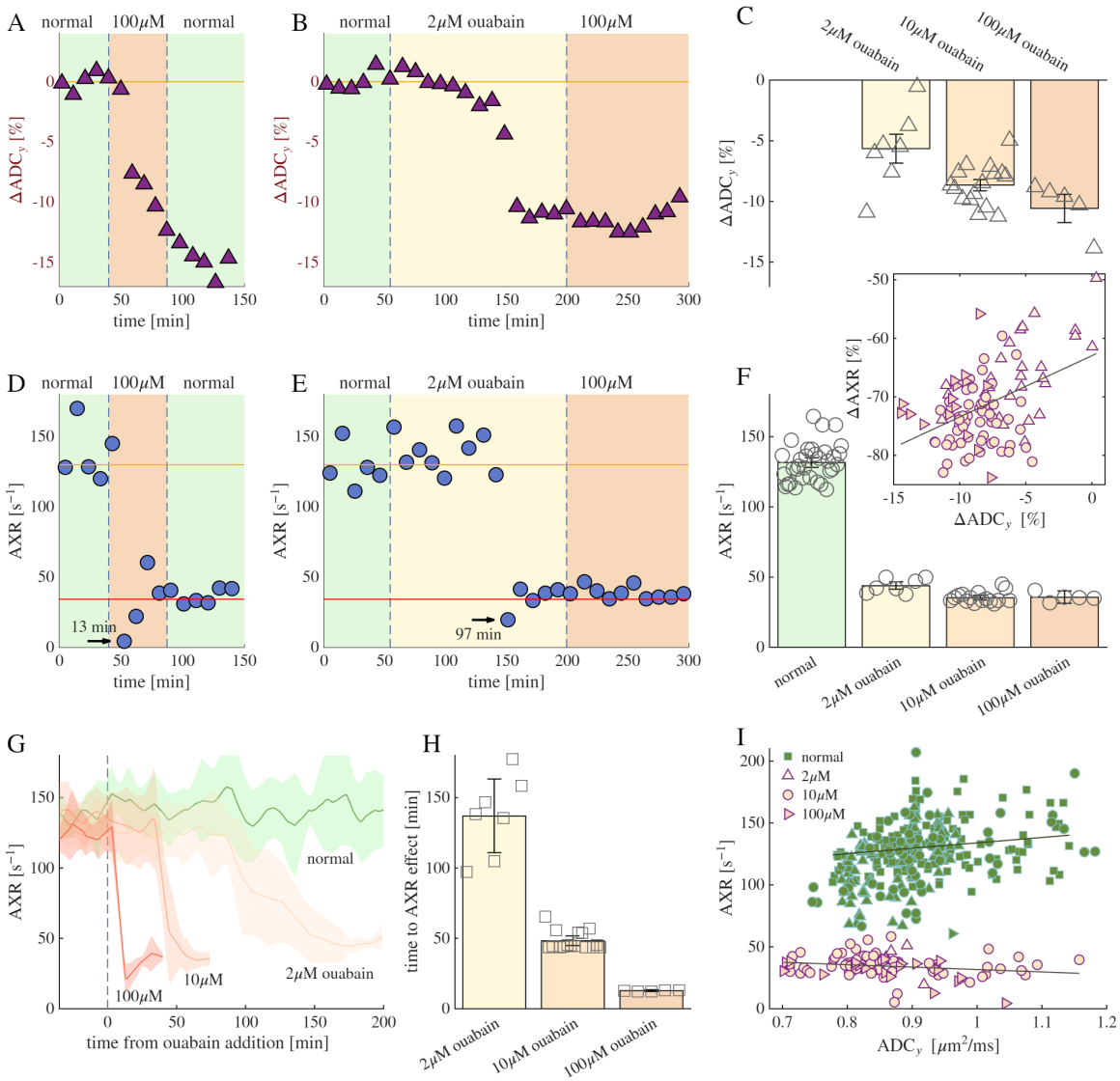

Fig. 1. Active ion transport inhibition has a large effect on AXR and simultaneously a smaller effect on ADC. A,B,D,E) Representative recordings on individual samples show how ouabain in (A,D) high (100 μM) and (B,E) low (2 μM) concentrations affects (A,B) ADC in the y-direction (presented as % change from baseline, $\Delta\mathrm{ADC}_y$) and (D,E) AXR. In (D) and (E), arrows and text show when AXR decreased below 60 s^{-1} and the time from ouabain addition to the effect. C,F) Bar graphs of (C) $\Delta\mathrm{ADC}_y$ and (F) AXR, showing the mean across all measurements (bar height), 95% CI of the mean (whiskers), and mean values from each sample (open symbols) for normal, 2, 10, and 100 μM ouabain conditions (n =33, 7, 16, and 5, respectively). For ouabain conditions, data was compiled from the first 3 to 5 measurements after an effect was observed and did not incorporate data from additional treatments or doses. F-inset) The correlation between $\Delta\mathrm{ADC}_y$ and Δk for all measurements in the 2, 10, and 100 μM ouabain-treated groups (right-pointing triangles, circles, and up-pointing triangles, respectively). G) Mean (solid lines) and standard deviation (shaded regions) of AXR recordings from a control group under normal conditions (green) and groups treated with 2, 10, and 100 μM ouabain (lightest to darkest colors) plotted against the time after addition of ouabain. H) Bar chart of the time from ouabain addition to the time at which AXR dropped below 60 s^{-1}. I) Correlation plot of ADC_y vs. AXR. Data collected before ouabain treatment makes up the normal group (green squares), and data collected after ouabain treatment was further split into $\mathrm{AXR} < 60\ \mathrm{s}^{-1}$ (pink symbols, see legend) and $\mathrm{AXR} > 60\ \mathrm{s}^{-1}$ (same symbols, but green) groups. Additional metrics and correlations are presented in Fig. S1.

membrane exchange in this system does not have a significant active component on the 1–300 ms timescales probed by low-field, high gradient DEXSY.

AXR depends on tonicity. Next, we study the effects of osmolytes (sucrose and mannitol) on ADC_y and AXR under normal conditions as well as after ouabain administration. The Van't Hoff equation predicts linear relationships between intracellular and extracellular osmotic pressures (π_i and π_o) and osmolyte concentrations (c_i and c_o),

$$\pi_i = c_i RT \ \text{ and } \ \pi_o = c_o RT \tag{1}$$

where R is the ideal gas constant and T is the absolute temperature.[42] This relationship is valid for the dilute sucrose concentrations we study here,[43] although it may deviate from ideality when adding sucrose with biological solutes already present.[31,44] For reference, the Van't Hoff equation predicts +100 mOsm at 25°C (or 298.15 K) to increase π_o by +240 kPa. To reach a steady-state, this pressure must be balanced by an increase in π_i or hydrostatic pressures. In viable tissue,

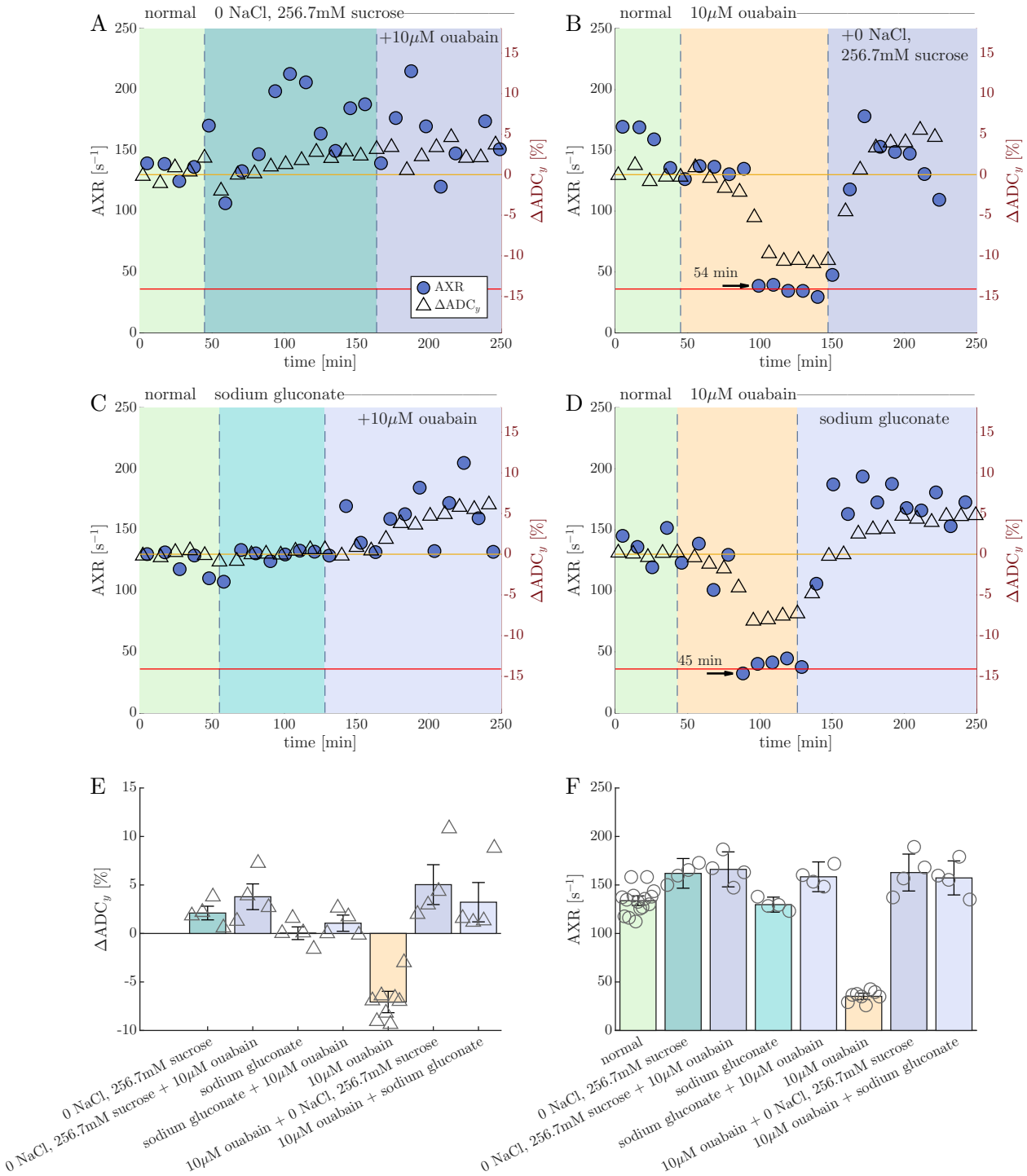

Fig. 2. AXR is not directly linked to ion transport, voltage, or active water cycling. A–D) Representative recording of AXR (blue circles) and % change in ADC_y (open triangles) during experiments involving (A,C) washing the sample from normal media to media in which NaCl was replaced with equiosmolar concentration of (A) sucrose (256.7 mM) or (C) sodium gluconate (128 mM), and then adding 10 μM ouabain, and (B,D) adding 10 μM ouabain on top of normal media, waiting for the effect, and then washing to (B) 0 NaCl, 256.7 mM sucrose media or (D) sodium gluconate media in the presence of 10 μM ouabain. E,F) Box plots of (E) $\Delta\mathrm{ADC}_y$ and (F) AXR showing the statistics across $n = 4$ samples.

π_i can increase by regulatory volume increase (RVI) mechanisms, which involve Na^+ and K^+ uptake coupled with electroneutral transport of Cl^-, in-part by reducing $\mathrm{Na}^+/\mathrm{K}^+$–ATPase activity.[41,45] Regardless of viability, cellular shrinkage causes an increase in intracellular osmotic pressure due to an increase in the concentration of trapped intracellular impermeants.[30]

First, the effect of +100 mOsm sucrose was observed on the same sample before and after adding 10 μM ouabain (Fig. 3). ADC_y followed trends expected for cellular shrinking and swelling; it increased in the +100 mOsm hypertonic conditions, recovered in normal isotonic media, and decreased slightly when ouabain took effect (Fig. 3A,B). In the context of AWC, increased osmolarity would be expected

to reduce Na^+/K^+–ATPase activity[45] and in this way reduce AXR. In contrast, starting from the normal condition, +100 mOsm increased AXR slightly but significantly ($p = 0.03$), by $14 \pm 25\%$. (Fig. 3C,D). The minimal effect here could be due to regulatory mechanisms maintaining tonicity despite increasing extracellular osmolarity.[41] After ouabain took effect, +100 mOsm increased AXR much more, by $233 \pm 68\%$. This further suggests AXR is related to the tonicity. AXR dropped back down when the osmolyte was washed away in the presence of ouabain (Fig. 3C,D).

Next, the effects of sucrose dosages in the range of +10 to +200 mOsm were studied on normal samples and on separate samples treated with 10 μM ouabain (Fig. 4A,B). On normal samples, ΔADC_y and AXR increased only slightly; the effect was insignificant for dosages up to +100 mOsm but became significant at +200 mOsm (Fig. 4A,C,E). For ouabain-treated samples, ΔADC_y and AXR increased significantly for doses between +30 mOsm and +100 mOsm. The trend changed at +200 mOsm, with ΔADC_y and AXR decreasing slightly, although not significantly (Fig. 4B,C,E). Comparing ΔADC_y and AXR between the normal and ouabain-treated groups, both values were significantly lower for ouabain-treated samples at +0 mOsm and similar between groups at +100 mOsm. At +200 mOsm, AXR of ouabain-treated samples was significantly less than that of normal samples (Fig. 4E) but ΔADC_y remained similar between sample groups (Fig. 4C). The effects of mannitol were also studied on ouabain-treated samples (Fig. 4D). Mannitol (MW= 182 g/mol) is a smaller molecule than sucrose (MW= 342 g/mol) and is also used as a cellular osmolyte.[27] Mannitol and sucrose increased ΔADC_y to similar values at each concentration (Fig. 4C). This is in spite of sucrose reducing the ADC of pure aCSF media to a greater degree than mannitol due to its greater effect on fluid viscosity (Fig. S4). Thus the compounds' osmotic effects (cell shrinkage increasing ADC_y) are more significant than their viscous effects (reducing ECS diffusivity). Their viscous effects may become apparent at higher concentrations, e.g. at 200 mM, where the average ADC of samples treated with sucrose is less than those treated with mannitol, although not significantly. Mannitol and sucrose also increased AXR similarly across concentrations (Fig. 4E). This indicates that their effect on AXR is osmotic in nature.

We tested whether the effects of osmolytes were similar or different between normal and ouabain-treated groups by examining correlations between ΔADC_y and ΔAXR (Fig. 4F). The two groups have different correlations and occupy distinct regions of the plot (see distinct model fits and 95% CI). Data from normal samples appears clustered due to osmolytes having very little effect. For ouabain-treated samples, ΔADC_y and ΔAXR show a sigmoidal relationship, being highly correlated at intermediate ΔADC_y and weakly correlated at low and high ΔADC_y. This behavior is not due to measurement insensitivity because we report lower AXR's for ouabain-treated samples at 11°C (Fig. 5E) and we previously reported higher AXR's for normal samples at 35°C (in Fig. 1B of Ref. 12).

Osmotic perturbations with 100 mM sucrose and with variable concentrations up to 200 mM yielded consistent results overall (Fig. 4C,E). Differences were observed during the wash from hypertonic media to normal media on samples not treated with ouabain. AXR recovered to stable values slightly below baseline after washing out the +100 mOsm solution, but dropped to low levels, similar to ouabain-treated values, after washing out the +200 mOsm solution. (compare Fig. 3C to Fig. 4A). It appears that the samples maintained homeostasis during the wash in the first case but not in the second. This could be because of the larger osmotic change in combination with a longer experiment time. 200 mM is more than cell RVI mechanisms can physiologically balance given the limited NaCl and KCl in the aCSF and may have damaged the cells. Additionally, intracellular penetration of sucrose may have caused rebound swelling when washed to normal media. For reference, the wash occurred at roughly 120 minutes in the 100 mM case and at roughly 300 minutes in the 200 mM case.

While osmolytes restore AXR of ouabain-treated samples to baseline levels, it is unclear whether the same exchange pathways are recovering or if SVR changes are responsible. Measuring activation energies from the temperature dependence of AXR can help distinguish these causes, as they reflect the energy barriers of underlying water exchange pathways, they do not depend on SVR differences between sample groups, and they can be compared across studies.[17]

Tonicity affects activation energies of exchange but not of diffusion. Here, we study samples under normal conditions, treated with 10 μM ouabain, treated with 100 mM sucrose, and treated with 10 μM ouabain + 100 mM sucrose. For each condition, AXR and ADC_y was recorded at 25°C and 11°C, and re-recorded at 25°C to test for sample recovery (Fig. 5A–E). AXR recovered when re-recorded at 25°C (one-way ANOVA, $p > 0.05$). The dependence of AXR on the absolute temperature T is modeled with the Arrhenius equation

$$k = A\exp(-E_a/RT) \quad \textbf{(2)}$$

where A is the pre-exponential factor, E_a is the activation energy, and R is the ideal gas constant (Fig. 5F). While deviations from Arrhenius behavior are hidden when only two temperatures are studied, we tested for this in a previous study and found the Arrhenius model to fit well for normal and fixed spinal cords at 7, 25, and 35 °C.[12] E_a values for exchange are similar between the normal samples ($E_a = 42.6 \pm 6.4$ kJ/mol) and normal +100 mOsm samples (43.2 ± 2.8 kJ/mol), but different from the ouabain-treated samples (25.2 ± 0.8 kJ/mol, Fig. 5H). E_a recovers to 38.5 ± 1.6 kJ/mol when +100 mOsm is added to ouabain-treated samples, indicating that the recovery is related to tonicity but not directly related to Na^+/K^+–ATPase activity. Since E_a values are independent of SVR, this also indicates that the major effect of tonicity on AXR is not directly through SVR changes.Since SVR does not affect E_a, the difference in E_a between normal and ouabain-treated samples implies that changes in SVR alone can not explain the

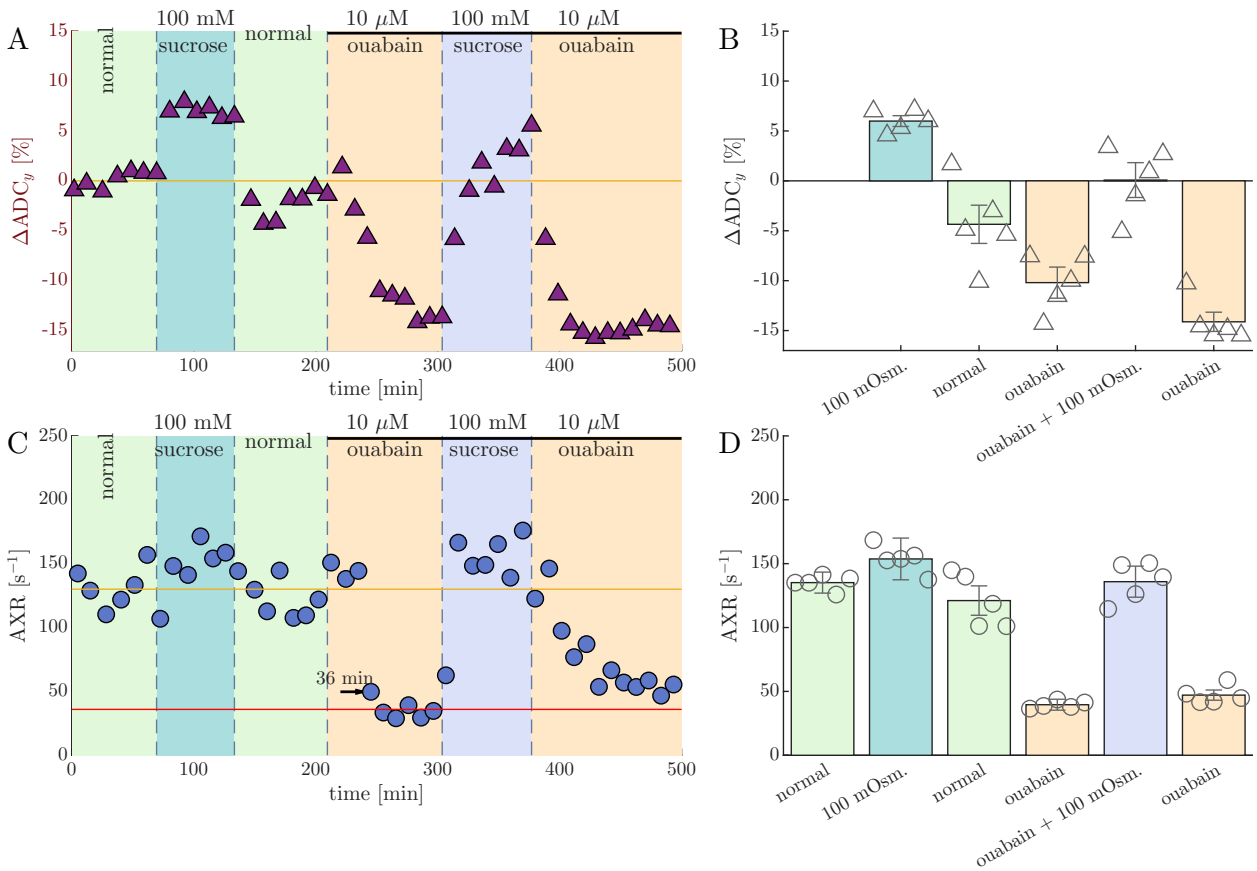

Fig. 3. Osmolytes recover AXR. A,C) Representative recordings of of (A) % change in $\mathrm{ADC_y}$ and (C) AXR during perturbations with 100 mM sucrose (an osmolyte) before and after the addition of 10 μM ouabain. The presence of 10 μM ouabain is shown by the solid-black line. B,D) Bar graphs showing the statistics across $n = 5$ samples.

changes in AXR observed. Faster AXR is associated with higher E_a (compare Fig. 5E,H). This is unexpected if these AXR pathways run in parallel between the same two compartments because the higher E_a means higher energy barriers which one would think to reduce exchange rate constants. Later, we show that this can arise in multi-site exchange with exchange pathways of differing activation energy.

Temperature affects water's thermal motion and self-diffusion coefficient.[46] In tissue, as temperature increases, the diffusion length scale and number of interactions with membrane surfaces increase. The ADC still goes up with temperature, but not as much as it would if diffusion were unimpeded, leading to the E_a being artificially reduced from that of pure water or an aqueous solution.[12] Indeed, values were lower than the value found for water self-diffusion in artificial cerebrospinal fluid (aCSF, $E_a = 18$ kJ/mol).[12] Nonetheless, comparisons between conditions is still valid.

In contrast to AXR, the Arrhenius analysis of ADC_y yielded similar E_a values between conditions (Fig. 6). This is consistent with the variability in ADC_y between conditions being simply related to microstructural effects like cellular swelling and shrinking and not to different diffusion mechanisms.

Exchange rate constants increasing with activation energy follows enthalpy–entropy compensation. As stated earlier, from a perspective of passive exchange between two sites, it is difficult to explain the increase of exchange E_a and AXR. For instance, if AXR increased due to an increase in membrane permeability, we would expect E_a to decrease. While SVR differences can affect AXR,[16] they should not affect exchange E_a.

In general kinetic phenomena, this behavior can arise when the overall rate constant depends on multiple competing pathways with different activation energies[47,48] and when the relative contributions of these pathways can be modulated by an additional component.[49] This behavior leads to a common linear dependence between E_a and the natural log of A across conditions

$$\ln(A) = m \times E_a + \ln(A'). \quad \textbf{(3)}$$

This is termed enthalpy–entropy compensation (EEC) because the activation energy E_a and the pre-exponential factor A are related to the enthalpy and entropy of the rate processes, respectively.[47,49–53] EEC implies that the system under any condition can be described by a modified Arrhenius model of the form

$$k = A' \exp\left(-E_a/R\,(1/T - 1/T_c)\right) \quad \textbf{(4)}$$

with a common crossover temperature $T_c = 1/(m \times R)$ at which AXR values are equal to A'.[50,53] Consistent with EEC, the E_a and $\ln(A)$ values were found to be linearly related through Eq. 3 across all conditions (Fig. 7A). This led to estimates of $T_c = -17°\mathrm{C}$ and $A' = 9.5\ \mathrm{s}^{-1}$ which, when

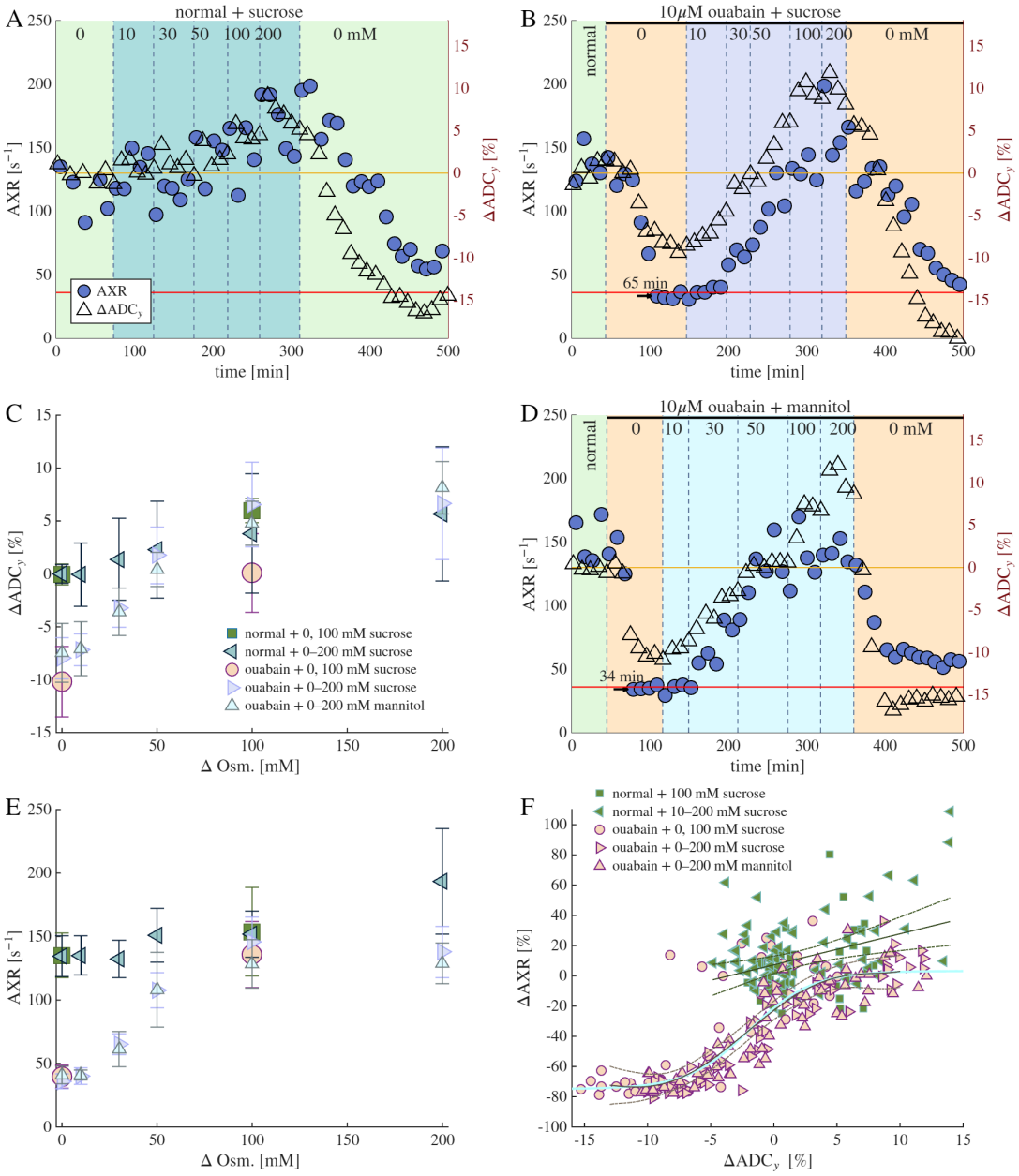

Fig. 4. AXR depends on tonicity. A,B,D) Recordings of AXR (left y-axis) and $\Delta\mathrm{ADC}_y$ (right y-axis) during osmotic perturbations with (A,B) sucrose or (D) mannitol concentrations 0, 10, 30, 50, 100, 200 mM and back to 0 mM on representative samples (A) starting from normal and (B,D) in the presence of 10 $\mu\mathrm{M}$ ouabain (shown by solid-back line). C,E) The effect of osmolarity on the mean (symbols) and standard deviations (error bars) of (C) ADC_y and (E) AXR when adding sucrose to samples under normal conditions ($n = 3$), and when adding sucrose ($n = 3$) or mannitol ($n = 3$) to samples treated with 10 $\mu\mathrm{M}$ ouabain (see legend in C). Data from Fig. 3 involving the addition of 100 mM sucrose in a single step pre-ouabain treatment and post-ouabain treatment are also shown. F) The correlation between $\Delta\mathrm{ADC}_y$ and Δk for all measurements performed on all samples in each group (see legend). Predicted means (solid lines) and 99% CI (broken lines) were found by regression of 1st order (combined normal samples) and 5th order (combined ouabain-treated samples) polynomials, with the latter being compared to a sigmoidal logistics function (aqua blue line). Additional metrics and correlations are presented in Fig. S5.

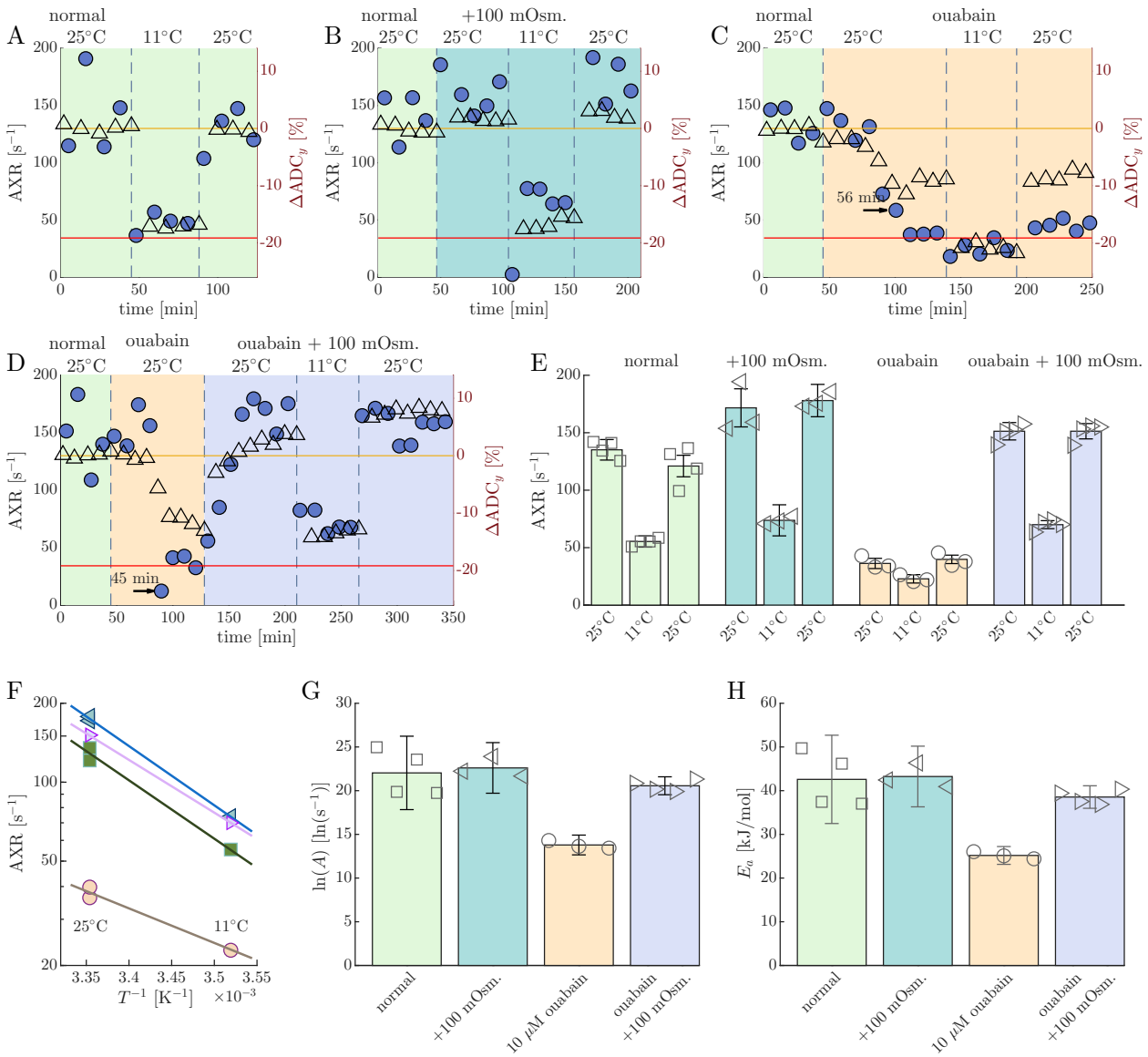

Fig. 5. Tonicity affects activation energies of exchange. A–D) Recordings of AXR (blue circles) and $\Delta\mathrm{ADC}_y$ (open triangles) during temperature perturbation from 25°C to 11°C back to 25°C under (A) normal, (B) +100 mM sucrose, (C) 10 μM ouabain, (D) and 10 μM ouabain +100 mM sucrose conditions. E) Results of AXR recorded at 25°C, 11°C, and again at 25°C on samples under normal ($n = 4$), +100 mOsm ($n = 3$), 10 μM ouabain ($n = 3$), and 10 μM ouabain +100 mOsm ($n = 4$) conditions. F) Arrhenius plot of the inverse of the absolute temperature T^{-1} vs. the average AXR for each condition. Solid lines show average fits of the Arrhenius model (Eq. 2). The slope of the line on the semi-log plot is proportional to E_a. (Refer to error bars in E, G, and H for standard deviations of AXR and Arrhenius model parameters.) G,H) Bar graph of (G) the natural log of pre-exponential factor A and (H) activation energy E_a estimated from Arrhenius model fits.

put into Eq. 4, describes the temperature dependence of AXR for all systems (Fig. 7B). Appearance of EEC suggests a common mechanism exists under all conditions, where E_a and A are a function of tonicity alone.[47]

While other explanations for EEC remain possible, we propose a multi-site exchange mechanism in which tonicity modulates AXR and the overall activation energy by shifting ECS and ICS volume fractions, thereby changing the relative prominence of exchange pathways with distinct kinetics and activation energies.[29] We test this hypothesis by simulating temperature-dependent DEXSY data using a three-site exchange model (3XM) with exchange between an ECS compartment and two ICS compartments (Fig. 8) (See Methods and Ref 29). In the model, transmembrane exchange between ECS and ICS is assigned a faster rate constant with a higher activation energy, whereas geometric exchange between ICS compartments (k_g) is slower and has a lower activation energy. Tonicity alters ECS and ICS fractions via osmotic balance, which in turn changes DEXSY's sensitivity to each pathway. Intuitively, sensitivity to any exchange pathway depends on the signal fractions of the exchanging compartments involved. Decreased ECS volume fraction reduces the sensitivity to transmembrane exchange, shifting sensitivity towards geometric exchange. As ECS volume fraction increases, sensitivity shifts toward the fast, high-E_a transmembrane pathway, causing both AXR and its apparent activation energy to increase together. Under these conditions, the 3XM reproduces the observed EEC behavior, including similar values of T_c and A' (Fig. 7C,D). Although T_c lies below 0°C and cannot be experimentally accessed, 3XM simulations show

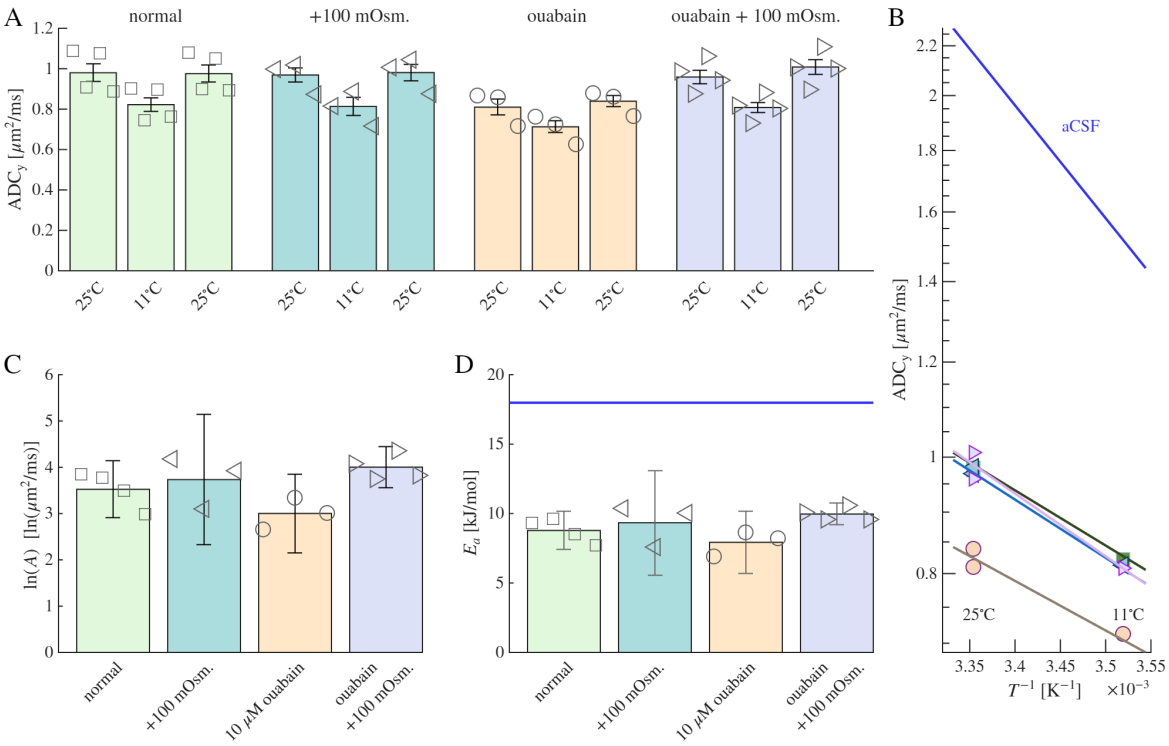

Fig. 6. Tonicity does not affect activation energies of diffusion. A) Results of $\mathrm{ADC_y}$ recorded at 25°C and 11°C and re-recorded at 25°C on samples under normal conditions ($n = 4$), after addition of 100 mM sucrose ($n = 3$), after the effect of 10 μM ouabain ($n = 3$), and after the combined effect of 10 μM ouabain and 100 mM sucrose ($n = 3$). B) Arrhenius plot of the inverse of the absolute temperature T^{-1} vs. the average $\mathrm{ADC_y}$ for each condition and for aCSF (reproduced from Ref. 12). Solid lines show average fits of the Arrhenius model (similar form to Eq. 2). C) Bar graph of the natural log of pre-exponential factor estimates. D) Bar graph of activation energy estimates, compared to the value for aCSF (blue line).

AXR converging at this point, where $\mathrm{AXR} = k_t = k_g = A'$ (Fig. 7D).

Independent of the 3XM's validity, EEC was able to describe AXR of all samples at all tonicities and temperatures, implying a model to estimate tonicity from AXR. In the Supporting Information, we develop this model by following Psurek *et al.* (2008).[49] and calibrate it using data from the ouabain and ouabain + 100 mOsm conditions. For normal samples, the model predicts $\Delta c = 90$ mOsm. This closely matches the $+82$ mOsm required to restore AXR in ouabain-treated samples, as determined by a linear fit of AXR versus sucrose concentration in Fig. 4E (line not shown). We interpret this as the change in tonicity associated with partitioned ions or, equivalently, intracellular impermeants and their countercations. Since no established method directly measures tonicity inside intact neural tissue, it is unfortunately not possible to validate this.

Discussion

$\mathrm{Na^+/K^+}$–ATPase inhibition by ouabain is considered a model for anoxic terminal depolarization of membrane potential[54,55] which often occurs during traumatic brain injury and stroke.[56] During terminal depolarization, ions and water redistribute between the ICS and ECS, leading to hypotonicity, cell swelling, and dramatic ECS shrinkage.[57,58] The "all-or-none" instability occurs at the point when $\mathrm{Na^+/K^+}$–ATPase activity no longer balances the $\mathrm{K^+}$ efflux. This creates a positive feedback loop with increasing extracellular $[\mathrm{K^+}]$ causing neuronal firing and additional $\mathrm{K^+}$ efflux. The

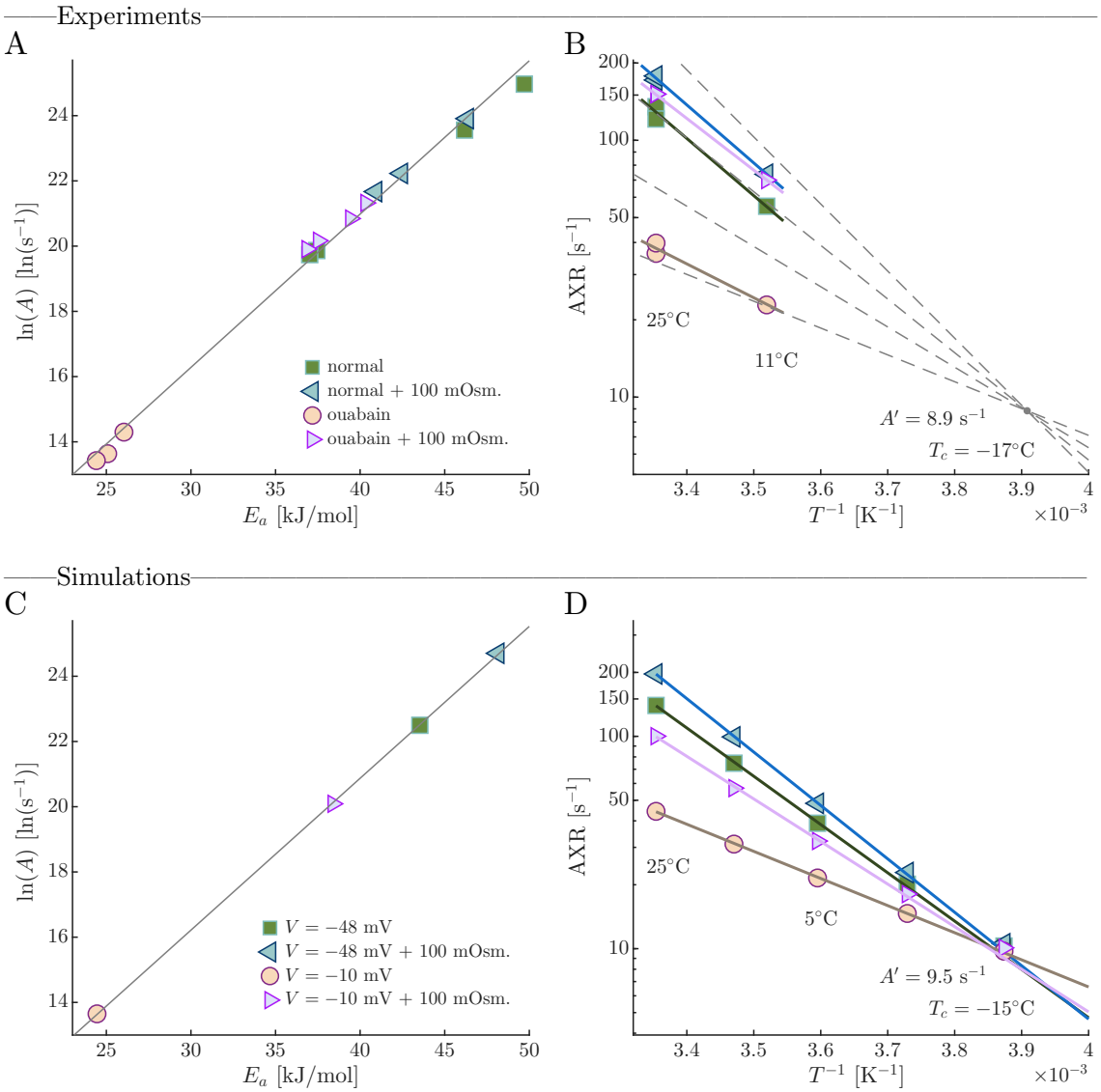

Fig. 7. Exchange rate constants increasing with activation energy follows enthalpy–entropy compensation A) Experimental activation energies plotted vs. the natural log of pre-exponential factors for all samples show a linear dependence described by Eq. 3 with slope $m = 0.470\ \ln(\mathrm{s}^{-1})/(\mathrm{kJ/mol})$ (95% CI = 0.447, 0.493) and y-intercept $\ln(A') = 2.18\ \ln(\mathrm{s}^{-1})$ (95% CI =1.30, 3.06). This is a sign of EEC and suggests a common crossover temperature $T_c = 1/(m \times R) - 273.15 = -17.1\,^{\circ}$C (-29,-4.3). B) Semi-log plot of Eq. 4 for a range of E_a (dashed lines) along with the data from Fig. 5F. C) E_a vs. $\ln(A)$ estimated from 3XM simulations. D) 3XM predictions of AXR at temperatures between -25 and $+25^{\circ}$C under voltage and osmolarity conditions modeling those studied experimentally (see legend in C). The modified Arrhenius model (Eq. 4) shows a common crossover temperature at $T_c = -15^{\circ}$C (-20,-9.2).

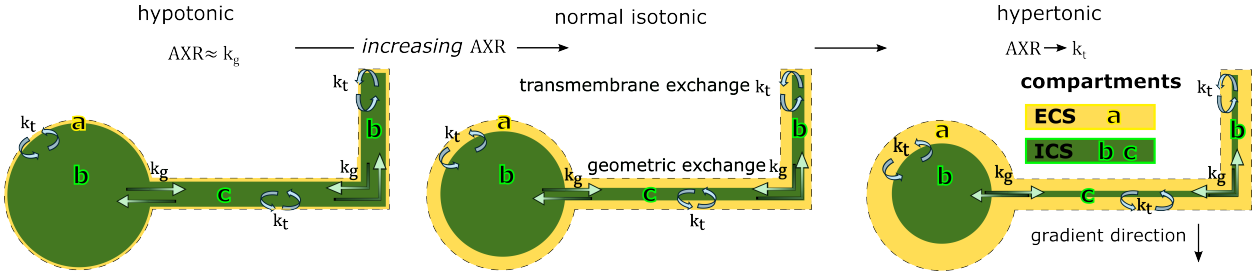

Fig. 8. Depiction of the connection between tonicity and AXR in a three-site exchange model (3XM) for gray matter. Compartment **a** represents the ECS. Compartment **b** represents cell soma and processes oriented parallel to the gradient direction where water appears more mobile. Compartment **c** represents cellular processes oriented perpendicular to the gradient direction where water appears less mobile. Transmembrane exchange k_t occurs between the ECS and ICS compartments. Geometric exchange k_g occurs between ICS compartments. Tonicity modulates AXR by changing the ECS fraction and the relative proportion of water seen exchanging with ECS.[29]

abrupt decrease in both AXR and ADC_y (Fig. 1) is likely a consequence of this. The 3XM explains why AXR is more dramatically affected than ADC_y (see Ref. 29). These findings suggest AXR may serve as a sensitive biomarker for spreading depolarization, potentially outperforming ADC alone.[59]

The effect of ouabain on AXR mirrors its impact on membrane potential observed by Balestrino *et al.*,[55] suggesting AXR and membrane potential are linked. However, separating the effects of tonicity and voltage with sodium gluconate and ouabain showed this link is indirect, mediated by changes in tonicity (Fig. 2).

Experiments decoupling tonicity from Na^+/K^+–ATPase activity showed that AWC is not significant in the *ex vivo* neonatal mouse spinal cord on 1–300 ms timescales. Inhibiting Na^+/K^+–ATPase activity did not reduce AXR when tonicity was maintained with impermeable osmolytes replacing semipermeable NaCl (Fig. 2). Osmolytes alone had little effect on AXR under normal conditions, despite likely reducing Na^+/K^+–ATPase activity,[45] but restored AXR under continued Na^+/K^+–ATPase inhibition (Figs. 3, 4). E_a recovered with AXR under conditions where AWC should not occur, suggesting that the same exchange mechanisms were restored through tonicity, but without involving AWC (Fig. 5).

Numerous studies suggest a link between water exchange and active ion transport.[7,12,18,19,22,44,60–65] While the 3XM could explain results of diffusion-based studies[7,12,22] it may not explain findings from studies using contrast agent-based methods[18,19,60–63,65] and on isolated cells[18,65] where geometric exchange is not expected. There is a discrepancy between our results and theirs, which we currently cannot explain. For contrast agent-based experiments, multisite exchange could still exist and changes in compartment volumes, even in the presence of contrast agents, can result in the appearance that transmembrane exchange is affected. To resolve this issue, experiments controlling for the effect of tonicity while perturbing activity should be performed. Combined diffusion- and contrast agent-based studies separating the effects of activity and tonicity will also help understand this discrepancy.

Our data revealed a positive, tonicity-dependent correlation between AXR and E_a, consistent with prior *ex vivo* studies comparing viable to fixed spinal cords[12] and viable to depolarized frog sciatic nerves.[60] The behavior was consistent with EEC. A model was developed based on EEC to estimate tonicity from AXR. While the model still needs further validation, the ability to non-invasively quantify tonicity in tissue is an important by-product of this work, since tonicity is a critical characteristic of the cellular state but is not measurable otherwise.

A multi-site exchange mechanism was introduced to explain the origin of EEC. We specified a three-site exchange model that includes geometric exchange between ICS regions and transmembrane exchange between ICS and ECS (Fig. 8).[29] Tonicity alters ECS volume fraction and hence the fraction of water molecules which DEXSY encodes as exchanging between ECS and ICS. This shifts the sensitivity of AXR between slower, low-E_a geometric exchange when the ECS fraction is smaller, and faster, high-E_a transmembrane exchange when the ECS fraction is larger.

The slower exchange has $E_a \approx 25\ \mathrm{kJ/mol}$, similar to water self-diffusion $E_a \approx 20\ \mathrm{kJ/mol}$ in pure water[46] and $E_a \approx 18\ \mathrm{kJ/mol}$ in aCSF. This is expected for geometric exchange involving hindered diffusion between intracellular compartments. Given the predominance of gray matter[66,67] and known microstructural features of the neonatal mouse spinal cord,[68,69] such exchange could occur along branched cellular processes[21] or between soma and processes.[70,71]

In contrast, the faster, but still passive exchange corresponds to a higher $E_a \approx 40\ \mathrm{kJ/mol}$. This value is indicative of transmembrane water exchange, and not geometric exchange. Potential pathways for transmembrane exchange include channels, cotransporters, and the lipid bilayer. Water channels such as aquaporin would reduce E_a towards $20\ \mathrm{kJ/mol}$[72] and hence play a minimal role. Ion cotransporters were also ruled out since it was shown by replacing NaCl with sucrose that it's the tonicity and not the ions themselves that are important. The E_a value is consistent with passive diffusion across lipid bilayers.[25] With no other high E_a pathways existing in high abundance, we conclude the lipid bilayer to be the dominant transmembrane exchange pathway on 1 to 300 ms timescales in this system.

This mechanism is quantitatively plausible. Geometric exchange rate constants should be relatively slow, based on timescales for diffusion across typical branching processes (e.g ≈ 0.1 to $80\ \mathrm{s}^{-1}$ for 5 to 145 μm branch lengths[28]) or for diffusion escape from soma to processes (e.g., $\approx 15\ \mathrm{s}^{-1}$ using Eq. 10 in Ref. 73 with an average 7 μm radius soma connected to six 0.8 μm radius processes[28]). Exchange between different cells, requiring at least two membrane crossings, may also be slow and appear geometric if diffusion through the cytosol is rate-limiting. In comparison transmembrane exchange rate constants are fast and predicted to exceed 100 s^{-1}, based on SVRs of 4 to 16 $\mu\mathrm{m}^{-1}$ in gray matter,[28] and permeabilities ranging from 70 to 400 $\mu\mathrm{m/s}$ for polyunsaturated membranes and decreased by about 50% with 40% cholesterol content,[25,26].

The 3XM predicts ADC and AXR to both depend on ECS volume fraction. We found ADC to correlate linearly with volume fraction metrics, but AXR showed a complex correlation (Figs. S1 and S5). Experiments show that ADC and AXR hold unique information during physiological vs. pathological cell swelling and shrinking (Fig. 4F). In essence ADC measures the global average of ADCs in every compartment, whereas AXR is related to volume fractions and eigenvalues of the exchange matrix.[29] While more possibilities exist, one explanation for this discrepancy between the 3XM and experiments is that the tissue contains more than three sites, and volume fractions are affected differently by perturbations under physiological vs pathological conditions. At this point, we believe that ADC and AXR are reporting different aspects of cell swelling.

These findings position DEXSY NMR as a powerful, noninvasive tool for probing steady-state water exchange and its biophysical and physiological underpinnings in viable tissue. More work is needed to understand the generality of these findings to more conventional gradient strengths and the *in vivo* human brain.[2–5] Nonetheless, future work is motivated by the possibility to infer tonicity and tissue state from combined measurements of AXR and ADC, to pro-

vide new biomarkers for monitoring normal function, development, aging, disease, and trauma without the need for contrast agents.

Methods

Details of NMR and tissue preparation methods can be found in Refs. 11,74, and 12, and are described briefly here.

Ethics statement for animal experimentation. All experiments were carried out in compliance with the *Eunice Kennedy Shriver* National Institute of Child Health and Human Development Animal Care and Use Committee under Animal Study Proposal (ASP) # 21-025.

Mouse spinal cord sample preparation and experimental conditions. All experiments were performed on Swiss Webster wild type mice (Taconic Biosciences, Rensselaer, NY, USA) between postnatal day 1 and 4. The mouse spinal cords were isolated in a dissecting chamber perfused with low-calcium, high-magnesium artificial cerebrospinal fluid (aCSF), with the same composition as normal aCSF (listed below) but 0.5 mM $CaCl_2 \cdot 2H_2O$ and 6 mM $MgSO_4 \cdot 7H_2O$, bubbled with 95% O_2/5% CO_2. After dissection, the spinal cord was placed in a radiofrequency (RF) coil in the sample chamber in normal calcium aCSF, composed of 128.35 NaCl, 4 KCl, 1.5 $CaCl_2 \cdot 2H_2O$, 1 $MgSO_4 \cdot 7H_2O$, 0.58 $NaH_2PO_4 \cdot H_2O$, 21 $NaHCO_3$, 30 D-glucose (concentrations in mM), bubbled with 95% O_2 and 5% CO_2 (for details, see Refs. 11,12). aCSF flowed through the chamber at 7 mL/min. Stock solutions of the pharmacological Na^+/K^+–ATPase inhibitor ouabain (European Pharmacopeia Reference Standard) and osmolytes sucrose or mannitol (Sigma Aldrich) were prepared in media and added to the media reservoir to reach desired concentrations. Washing to media in which the 128.35 mM NaCl was replaced with 256.7 mM sucrose or 128.35 mM sodium gluconate (Sigma Aldrich) or back to normal aCSF media involved washing in an open loop with 100 mL of new media. Sample temperature was monitored by a fiber optic sensor (PicoM, Opsens Solutions Inc., Québec, Canada) and controlled by a chiller that circulated water through the chamber base and a heat exchanger jacketed around the media tubing. The sample temperature was maintained at $25 \pm 0.2°$C by manually regulating the chiller temperature. Temperature perturbations were performed by switching to a second chiller which maintained the sample at $11 \pm 0.2°$C (5 min equilibration).

NMR hardware, experimental protocol, and analysis methods. NMR experiments were performed with a single-sided permanent magnet[75] (PM10 NMR MOUSE, Magritek, Aachen Germany) at magnetic field strength $B_0 = 0.3239$ T and gradient strength $g = 15.3$ T/m.

NMR experimental protocols involved looping through sets of diffusion experiments, rapid diffusion exchange experiments, and T_1 saturation recovery experiments. Each set took 11 minutes to acquire. Diffusion experiments were performed using a standard spin echo sequence[76] and 4-step phase cycle.[77] The encoding time, τ of the spin echo was varied linearly from 0.05 to 3.3 ms over 22 steps with 4 scans per τ. This corresponds to b-values ranging from 0.001 to 400 $\mathrm{ms}/\mu\mathrm{m}^2$ where $b = 2/3\gamma^2 g^2 \tau^3$ and γ is the gyromagnetic ratio.[78] Points two through four ($\tau = 0.2048$ to 0.5143 ms, $b = 0.096$ to $1.5\ \mathrm{ms}/\mu\mathrm{m}^2$) of diffusion data were fit with $I(b) = I_0 \exp(-b\,\mathrm{ADC})$ to estimate the ADC and I_0, the NMR signal in the absence of diffusion weighting. For measurements on spinal cords, the term ADC_y is used, acknowledging that diffusion may be anisotropic but was measured only along the y direction, perpendicular to the cord.

Rapid diffusion exchange experiments were performed following the Diffusion Exchange Ratio (DEXR) method[79] using a DEXSY sequence involving two spin echoes separated by a mixing time t_m in the presence of a static magnetic field gradient.[11] A 4-step phase cycle selects only the desired DEXSY coherence transfer pathway.[80] Experiments were performed with (τ_1, τ_2) combinations (0.200, 0.735) ms and (0.593, 0.580) ms, 8 scans per combination, and t_m values [0.2, 1, 2, 4, 7, 10, 20, 40, 80, 160, 300] ms. The signals from $(\tau_1, \tau_2) =$ (0.200, 0.735) were fit with a biexponential relaxation model. The $(\tau_1, \tau_2) =$(0.593, 0.580) signals were divided by the biexponential relaxation model and then fit with $I(t_m) = I_0 \exp(-t_m \mathrm{AXR}) + B$ to estimate the apparent exchange rate constant, AXR (similar to Method 3 in Ref. 74).

Hypothesis tests of whether NMR metrics were affected by perturbations were performed using paired-sample t-tests. Two-sample t-tests were used to determine whether means of treatment groups were significantly different. Tests for ADC and AXR recovery were performed using one-way ANOVA. $p < 0.05$ was deemed as significant.

Simulation methods. The pump–leak model (PLM) of cell volume maintenance provided by Kay (2017) was used to predict how perturbations affect cell volume and transmembrane voltage.[30] Additionally, a three-site exchange model (3XM) was developed to predict how perturbations affect the ECS fraction (f_o), ADC, and AXR. These models are detailed in Ref. 29, with key information provided here and in the Supporting Information.

In the 3XM, volume fractions are defined based on an osmolarity balance and fixed total volume (Eq. S8). The osmolarity balance includes trapped impermeants (i.e., solutes which are trapped in the ECS or ICS and can not cross the plasma membrane or communicate with the bathing media), small osmolytes (i.e., solutes in the ECS that can not cross the plasma membrane but can communicate with the bathing media), and ions partitioned by the voltage. We used -48 mV to model normal conditions (based on intracellular recordings in the *ex vivo* neonatal mouse spinal cord model[81]) and -10 mV to model Na^+/K^+–ATPase inhibition by ouabain (based on recordings in CNS under hypoxic or terminal depolarization[57]). The initial f_o for the normal condition was set to 0.3, (based on tetramethylammonium realtime iontophoresis measurements in a neonatal mouse spinal cord slice model[27,58]).

The three sites or compartments in the exchange model were

an ECS compartment and two ICS compartments with differing apparent mobilities. ADC was modeled as the sum of the ADC values of each compartment multiplied by their relative volume fractions.[82] AXR was modeled by simulating DEXSY data using an operator formalism[83–85] and then fitting the exchange model discussed above. The exchange operator involved an exchange matrix (Eq. S9) with rate constants for transmembrane exchange between ECS and ICS (k_t) and geometric exchange between ICS compartments (k_g) determined by the Arrhenius model (Eq. 2) using $E_a = 52\ \mathrm{kJ/mol}$ for k_t and $E_a = 22\ \mathrm{kJ/mol}$ for k_g, based roughly on the extremes of the experimental data, and A values were defined by Eq. 3 with $\ln(A') = 2.18\ \ln(\mathrm{s}^{-1})$ and $T_c = -17.1°\mathrm{C}$ found experimentally (presented in Fig. 7).

ACKNOWLEDGEMENTS

This work was partially funded by the Department of War in the Military Traumatic Brain Injury Initiative (MTBI^2) under award HU0001-24-2-0051. NHW, RR, TXC, and PJB were also supported by the IRP of the NICHD, NIH (Project numbers (PN): 1ZIAHD008971-07; 1ZIAHD008972-07). JAR was supported by an NIGMS Postdoctoral Research Associate Training (PRAT) Program Fellowship Award (PN: 1FI2GM150429-01; 1ZIEGM000002-18). We thank MJ O'Donovan and M Falgairolle for helpful discussions regarding the neonatal mouse spinal cord model, CS Springer and T Barbara for carefully reviewing the work, RW Pastor, AM Berezhkovskii, and SM Bezrukov for input on lipid membrane and channel permeability, and JF Douglas for bringing EEC to our attention.

CONTRIBUTIONS

Conceptualization, NHW, RR, TXC, JAR, and PJB; Methodology, NHW, RR, and TXC; Investigation, NHW and RR.; Writing – Original Draft, NHW; Writing – Review & Editing, NHW, RR, TXC, JAR, and PJB; Funding Acquisition, PJB; Supervision, PJB

DECLARATION OF INTERESTS

The authors have no financial interests to disclose. The views, information or content, and conclusions presented do not necessarily represent the official position or policy of, nor should any official endorsement be inferred on the part of, the Uniformed Services University, the Department of War, the U.S. Government or the Henry M. Jackson Foundation for the Advancement of Military Medicine, Inc.

DATA AND CODE AVAILABILITY

All data and code used to generate figures has been made publicly available at https://data.mendeley.com/datasets/rv3jmhb7wz

Bibliography

1. Nanna MacAulay. Molecular mechanisms of brain water transport. *Nature Reviews Neuroscience*, 22(6):326–344, 2021.
2. Arthur Chakwizira, Ante Zhu, Thomas Foo, Carl-Fredrik Westin, Filip Szczepankiewicz, and Markus Nilsson. Diffusion mri with free gradient waveforms on a high-performance gradient system: Probing restriction and exchange in the human brain. *NeuroImage*, 283:120409, 2023.
3. Quentin Uhl, Tommaso Pavan, Malwina Molendowska, Derek K Jones, Marco Palombo, and Ileana Ozana Jelescu. Quantifying human gray matter microstructure using neurite exchange imaging (nexi) and 300 mt/m gradients. *Imaging Neuroscience*, 2:1–19, 2024.
4. Dan Wu, Hong-Hsi Lee, Ruicheng Ba, Victoria Turnbill, Xiaoli Wang, Yu Luo, Piotr Walczak, Els Fieremans, Dmitry S. Novikov, Lee J. Martin, Frances J. Northington, and Jiangyang Zhang. In vivo mapping of cellular resolution neuropathology in brain ischemia with diffusion mri. *Science Advances*, 10(29):eadk1817, 2024. doi: 10.1126/sciadv.adk1817.
5. Kwok-Shing Chan, Yixin Ma, Hansol Lee, José P Marques, Jonas L Olesen, Santiago Coelho, Dmitry S Novikov, Sune N Jespersen, Susie Y Huang, and Hong-Hsi Lee. In vivo human neurite exchange time imaging at 500 mt/m diffusion gradients. *Imaging Neuroscience*, 2025.
6. Jörg Kärger, Harry Pfeifer, and Wilfried Heink. Principles and application of self-diffusion measurements by nuclear magnetic resonance. In *Advances in Magnetic and optical resonance*, volume 12, pages 1–89. Elsevier, 1988.
7. Charles S Springer Jr, Eric M Baker, Xin Li, Brendan Moloney, Gregory J Wilson, Martin M Pike, Thomas M Barbara, William D Rooney, and Jeffrey H Maki. Metabolic activity diffusion imaging (madi): I. metabolic, cytometric modeling and simulations. *NMR in Biomedicine*, 36 (1):e4781, 2023.
8. P. T. Callaghan and I. Furó. Diffusion-diffusion correlation and exchange as a signature for local order and dynamics. *The Journal of Chemical Physics*, 120(8):4032–4038, 2004.
9. Ying Qiao, Petrik Galvosas, Thorsteinn Adalsteinsson, Monika Schönhoff, and Paul T Callaghan. Diffusion exchange nmr spectroscopic study of dextran exchange through polyelectrolyte multilayer capsules. *The Journal of chemical physics*, 122(21):214912, 2005.
10. Denis S Grebenkov. Nmr survey of reflected brownian motion. *Reviews of Modern Physics*, 79(3):1077, 2007.
11. Nathan H Williamson, Rea Ravin, Dan Benjamini, Hellmut Merkle, Melanie Falgairolle, Michael James O'Donovan, Dvir Blivis, Dave Ide, Teddy X Cai, Nima S Ghorashi, et al. Magnetic resonance measurements of cellular and sub-cellular membrane structures in live and fixed neural tissue. *Elife*, 8:e51101, 2019.
12. Nathan H Williamson, Rea Ravin, Teddy X Cai, Melanie Falgairolle, Michael J O'Donovan, and Peter J Basser. Water exchange rates measure active transport and homeostasis in neural tissue. *PNAS nexus*, 2(3):pgad056, 2023.
13. Helene Benveniste, Laurence W Hedlund, and G Allan Johnson. Mechanism of detection of acute cerebral ischemia in rats by diffusion-weighted magnetic resonance microscopy. *Stroke*, 23(5):746–754, 1992.
14. Ingrid Åslund, Agnieszka Nowacka, Markus Nilsson, and Daniel Topgaard. Filter-exchange PGSE NMR determination of cell membrane permeability. *Journal of Magnetic Resonance*, 200(2):291 – 295, 2009. ISSN 1090-7807.
15. Xin Tian, Hua Li, Xiaoyu Jiang, Jingping Xie, John C Gore, and Junzhong Xu. Evaluation and comparison of diffusion mr methods for measuring apparent transcytolemmal water exchange rate constant. *Journal of Magnetic Resonance*, 275:29–37, 2017.
16. Dominik Ludwig, Frederik Bernd Laun, Mark Edward Ladd, Peter Bachert, and Tristan Anselm Kuder. Apparent exchange rate imaging: On its applicability and the connection to the real exchange rate. *Magnetic Resonance in Medicine*, 86(2):677–692, 2021.
17. AS Verkman. Water permeability measurement in living cells and complex tissues. *The Journal of membrane biology*, 173(2):73–87, 2000.
18. Yajie Zhang, Marie Poirier-Quinot, Charles S Springer Jr, and James A Balschi. Active trans-plasma membrane water cycling in yeast is revealed by nmr. *Biophysical journal*, 101 (11):2833–2842, 2011.
19. Ruiliang Bai, Charles S Springer Jr, Dietmar Plenz, and Peter J Basser. Fast, na+/k+ pump driven, steady-state transcytolemmal water exchange in neuronal tissue: A study of rat brain cortical cultures. *Magnetic Resonance in Medicine*, 79(6):3207–3217, 2018.
20. Charles S Springer Jr. Using 1h2o mr to measure and map sodium pump activity in vivo. *Journal of Magnetic Resonance*, 291:110–126, 2018.
21. Mohammad Khateri, Marco Reisert, Alejandra Sierra, Jussi Tohka, and Valerij G Kiselev. What does fexi measure? *NMR in Biomedicine*, 35(12):e4804, 2022.
22. Charles S Springer Jr, Eric M Baker, Xin Li, Brendan Moloney, Martin M Pike, Gregory J Wilson, Valerie C Anderson, Manoj K Sammi, Mark G Garzotto, Ryan P Kopp, et al. Metabolic activity diffusion imaging (madi): Ii. noninvasive, high-resolution human brain mapping of sodium pump flux and cell metrics. *NMR in Biomedicine*, 36(1):e4782, 2023.
23. Andreea Hertanu, Tommaso Pavan, and Ileana O Jelescu. Somatosensory-evoked response induces extensive diffusivity and kurtosis changes associated with neural activity in rodents. *Imaging Neuroscience*, 2025.
24. Clare Howarth, Padraig Gleeson, and David Attwell. Updated energy budgets for neural computation in the neocortex and cerebellum. *Journal of Cerebral Blood Flow & Metabolism*, 32(7):1222–1232, 2012.
25. Daniel Huster, Albert J Jin, Klaus Arnold, and Klaus Gawrisch. Water permeability of polyunsaturated lipid membranes measured by 17o nmr. *Biophysical journal*, 73(2):855–864, 1997.
26. John C Mathai, Stephanie Tristram-Nagle, John F Nagle, and Mark L Zeidel. Structural determinants of water permeability through the lipid membrane. *The Journal of general physiology*, 131(1):69–76, 2008.
27. Eva Syková and Charles Nicholson. Diffusion in brain extracellular space. *Physiological reviews*, 88(4):1277–1340, 2008.
28. Charlie Aird-Rossiter, Hui Zhang, Daniel C Alexander, Derek K Jones, and Marco Palombo. Decoding gray matter: large-scale analysis of brain cell morphometry to inform microstructural modeling of diffusion mr signals. *arXiv preprint arXiv:2501.02100*, 2025.
29. Nathan H Williamson, Rea Ravin, Teddy X Cai, Julian A Rey, and Peter J Basser. Passive water exchange between multiple sites can explain why apparent exchange rate constants depend on ionic and osmotic conditions in gray matter. *Magnetic Resonance Letters*, page 200225, 2025. ISSN 2772-5162. doi: https://doi.org/10.1016/j.mrl.2025.200225.
30. Alan R Kay. How cells can control their size by pumping ions. *Frontiers in cell and developmental biology*, 5:41, 2017.
31. Håkan Wennerström and Mikael Oliveberg. On the osmotic pressure of cells. *QRB discovery*, 3:e12, 2022.
32. William J Obrien, Jerry B Lingrel, and Earl T Wallick. Ouabain binding kinetics of the rat alpha two and alpha three isoforms of the sodium-potassium adenosine triphosphate. *Archives of Biochemistry and Biophysics*, 310(1):32–39, 1994.
33. Nathan H Williamson, Velencia J Witherspoon, Teddy X Cai, Rea Ravin, Ferenc Horkay, and Peter J Basser. Low-field, high-gradient nmr shows diffusion contrast consistent with localization or motional averaging of water near surfaces. *Magnetic Resonance Letters*, 2023.
34. Donald DF Loo, Thomas Zeuthen, Grischa Chandy, and Ernest M Wright. Cotransport of water by the na+/glucose cotransporter. *Proceedings of the National Academy of Sciences*, 93(23):13367–13370, 1996.
35. AK Meinild, DA Klaerke, DDF Loo, EM Wright, and T Zeuthen. The human na+–glucose cotransporter is a molecular water pump. *The Journal of Physiology*, 508(Pt 1):15, 1998.
36. Thomas Zeuthen and Nanna MacAulay. Cotransporters as molecular water pumps. *International review of cytology*, 215:259–284, 2002.
37. Thomas Zeuthen. Water-transporting proteins. *Journal of Membrane Biology*, 234(2):57–73, 2010.
38. N MacAulay and T Zeuthen. Water transport between cns compartments: contributions of aquaporins and cotransporters. *Neuroscience*, 168(4):941–956, 2010.
39. Jonathan T Ting, Tanya L Daigle, Qian Chen, and Guoping Feng. Acute brain slice methods for adult and aging animals: application of targeted patch clamp analysis and optogenetics. *Patch-clamp methods and protocols*, pages 221–242, 2014.
40. Michael Müller and George G Somjen. Intrinsic optical signals in rat hippocampal slices during hypoxia-induced spreading depression-like depolarization. *Journal of neurophysiology*, 82(4):1818–1831, 1999.
41. Thomas J Jentsch. Vracs and other ion channels and transporters in the regulation of cell volume and beyond. *Nature Reviews Molecular Cell Biology*, 17(5):293, 2016.

42. J. H. van't Hoff. Die rolle osmotischen drucks in der analogie zwischen losungen und gasen. *Zeitschrift fur physikalische Chemie*, 1:481–508, 1887.
43. Alessandro Grattoni, Manuele Merlo, and Mauro Ferrari. Osmotic pressure beyond concentration restrictions. *The Journal of Physical Chemistry B*, 111(40):11770–11775, 2007.
44. Charles S Springer Jr, Martin M Pike, and Thomas M Barbara. Metabolic energy is stored in a homeostatic trans-membrane water barochemical gradient. *The Journal of Membrane Biology*, pages 1–26, 2025.
45. DW Whalley, LC Hool, RE Ten Eick, and HH Rasmussen. Effect of osmotic swelling and shrinkage on na (+)-k+ pump activity in mammalian cardiac myocytes. *American Journal of Physiology-Cell Physiology*, 265(5):C1201–C1210, 1993.
46. R Mills. Self-diffusion in normal and heavy water in the range 1-45. deg. *The Journal of Physical Chemistry*, 77(5):685–688, 1973.
47. Wendell Q Sun. Dielectric relaxation of water and water-plasticized biomolecules in relation to cellular water organization, cytoplasmic viscosity, and desiccation tolerance in recalcitrant seed tissues. *Plant Physiology*, 124(3):1203–1216, 2000.
48. Ekaterina M Nestorovich, Vladimir A Karginov, Alexander M Berezhkovskii, V Adrian Parsegian, and Sergey M Bezrukov. Kinetics and thermodynamics of binding reactions as exemplified by anthrax toxin channel blockage with a cationic cyclodextrin derivative. *Proceedings of the National Academy of Sciences*, 109(45):18453–18458, 2012.
49. Tatiana Psurek, Christopher L Soles, Kirt A Page, Marcus T Cicerone, and Jack F Douglas. Quantifying changes in the high-frequency dynamics of mixtures by dielectric spectroscopy. *The Journal of Physical Chemistry B*, 112(50):15980–15990, 2008.
50. D Daoukaki-Diamanti, P_ Pissis, and G Boudouris. Depolarization thermocurrents in frozen aqueous solutions of mono-and di-saccharides. *Chemical physics*, 91(2):315–325, 1984.
51. A Anopchenko, Tatiana Psurek, David VanderHart, Jack F Douglas, and Jan Obrzut. Dielectric study of the antiplasticization of trehalose by glycerol. *Physical Review E*, 74(3): 031501, 2006.
52. Hiroyuki Sugimoto, Tsunehisa Miki, Kozo Kanayama, and Misato Norimoto. Dielectric relaxation of water adsorbed on cellulose. *Journal of Non-Crystalline Solids*, 354(27):3220–3224, 2008.
53. Marcus T Cicerone and Jack F Douglas. β-relaxation governs protein stability in sugar-glass matrices. *Soft Matter*, 8(10):2983–2991, 2012.
54. Trent A Basarsky, Steven N Duffy, R David Andrew, and Brian A MacVicar. Imaging spreading depression and associated intracellular calcium waves in brain slices. *Journal of Neuroscience*, 18(18):7189–7199, 1998.
55. Maurizio Balestrino, Jacob Young, and Peter Aitken. Block of (na+, k+) atpase with ouabain induces spreading depression-like depolarization in hippocampal slices. *Brain research*, 838(1-2):37–44, 1999.
56. Jens P Dreier. The role of spreading depression, spreading depolarization and spreading ischemia in neurological disease. *Nature medicine*, 17(4):439–447, 2011.
57. George G Somjen. Mechanisms of spreading depression and hypoxic spreading depression-like depolarization. *Physiological reviews*, 81(3):1065–1096, 2001.
58. Miroslava Anděrová, Šárka Kubinová, Tomáš Mazel, Alexandr Chvátal, Camilla Eliasson, Milos Pekny, and Eva Syková. Effect of elevated k+, hypotonic stress, and cortical spreading depression on astrocyte swelling in gfap-deficient mice. *Glia*, 35(3):189–203, 2001.
59. Lawrence L Latour, Yasuhiro Hasegawa, James E Formato, Marc Fisher, and Christopher H Sotak. Spreading waves of decreased diffusion coefficient lifter cortical stimulation in the rat brain. *Magnetic resonance in medicine*, 32(2):189–198, 1994.
60. OG Fritz Jr and TJ Swift. The state of water in polarized and depolarized frog nerves: A proton magnetic resonance study. *Biophysical Journal*, 7(6):675–687, 1967.
61. Charles S Springer Jr, Xin Li, Luminita A Tudorica, Karen Y Oh, Nicole Roy, Stephen Y-C Chui, Arpana M Naik, Megan L Holtorf, Aneela Afzal, William D Rooney, et al. Intratumor mapping of intracellular water lifetime: metabolic images of breast cancer? *NMR in Biomedicine*, 27(7):760–773, 2014.
62. William D Rooney, Xin Li, Manoj K Sammi, Dennis N Bourdette, Edward A Neuwelt, and Charles S Springer Jr. Mapping human brain capillary water lifetime: high-resolution metabolic neuroimaging. *NMR in Biomedicine*, 28(6):607–623, 2015.
63. Ruiliang Bai, Charles S Springer Jr, Dietmar Plenz, and Peter J Basser. Brain active transmembrane water cycling measured by mr is associated with neuronal activity. *Magnetic resonance in medicine*, 81(2):1280–1295, 2019.
64. Eleonora Cavallari, Elena Lorenzi, Enza Di Gregorio, Giuseppe Ferrauto, Silvio Aime, Giorgio Vallortigara, and Angelo Bifone. In vivo assessment of the influence of general anaesthetics on transmembrane water cycling in the brain. *Journal of Cerebral Blood Flow & Metabolism*, page 0271678X241309783, 2024.
65. Samantha Mumford. *Characterizing the Influence of Metabolism on Steady State Water Exchange in Yeast as a Potential MRI Diagnostic Biomarker*. PhD thesis, Portland State University, 2024.
66. Alex M Henry and John G Hohmann. High-resolution gene expression atlases for adult and developing mouse brain and spinal cord. *Mammalian genome*, 23(9-10):539–549, 2012.
67. Gulgun Sengul, Ralph B Puchalski, and Charles Watson. Cytoarchitecture of the spinal cord of the postnatal (p4) mouse. *The Anatomical Record: Advances in Integrative Anatomy and Evolutionary Biology*, 295(5):837–845, 2012.
68. Hui-Hsin Tsai, Huiliang Li, Luis C Fuentealba, Anna V Molofsky, Raquel Taveira-Marques, Helin Zhuang, April Tenney, Alice T Murnen, Stephen PJ Fancy, Florian Merkle, et al. Regional astrocyte allocation regulates cns synaptogenesis and repair. *Science*, 337(6092): 358–362, 2012.
69. Dvir Blivis, Melanie Falgairolle, and Michael J O'Donovan. Dye-coupling between neonatal spinal motoneurons and interneurons revealed by prolonged back-filling of a ventral root with a low molecular weight tracer in the mouse. *Scientific Reports*, 9(1):1–9, 2019.
70. Marco Palombo, Andrada Ianus, Michele Guerreri, Daniel Nunes, Daniel C Alexander, Noam Shemesh, and Hui Zhang. Sandi: a compartment-based model for non-invasive apparent soma and neurite imaging by diffusion mri. *Neuroimage*, 215:116835, 2020.
71. Andrada Ianus, Daniel C Alexander, Hui Zhang, and Marco Palombo. Mapping complex cell morphology in the grey matter with double diffusion encoding mr: A simulation study. *Neuroimage*, 241:118424, 2021.
72. Philip W Kuchel and Gheorghe Benga. Why does the mammalian red blood cell have aquaporins? *Biosystems*, 82(2):189–196, 2005.
73. Denis S Grebenkov, Ralf Metzler, and Gleb Oshanin. Full distribution of first exit times in the narrow escape problem. *New Journal of Physics*, 21(12):122001, 2019.
74. Nathan H Williamson, Rea Ravin, Teddy X Cai, Dan Benjamini, Melanie Falgairolle, Michael J O'Donovan, and Peter J Basser. Real-time measurement of diffusion exchange rate in biological tissue. *Journal of Magnetic Resonance*, 317:106782, 2020.
75. G Eidmann, R Savelsberg, Peter Blümler, and Bernhard Blümich. The nmr mouse, a mobile universal surface explorer. *Journal of Magnetic Resonance*, 122:104–109, 1996.
76. D.G. Rata, F. Casanova, J. Perlo, D.E. Demco, and B. Blümich. Self-diffusion measurements by a mobile single-sided nmr sensor with improved magnetic field gradient. *Journal of Magnetic Resonance*, 180(2):229 – 235, 2006. ISSN 1090-7807. doi: https://doi.org/10.1016/j.jmr.2006.02.015.
77. Federico Casanova, Juan Perlo, and Bernhard Blümich. *Single-sided NMR*. Springer, 2011.
78. Erwin L Hahn. Spin echoes. *Physical review*, 80(4):580, 1950.
79. Teddy X Cai, Nathan H Williamson, Rea Ravin, and Peter J Basser. The diffusion exchange ratio (dexr): A minimal sampling of diffusion exchange spectroscopy to probe exchange, restriction, and time-dependence. *Journal of Magnetic Resonance*, page 107745, 2024.
80. Teddy Xuke Cai. *In search of lost time: development of rapid magnetic resonance methods to probe time-varying diffusion*. PhD thesis, University of Oxford, 2023.
81. Melanie Falgairolle, Joshua G Puhl, Avinash Pujala, Wenfang Liu, and Michael J O'Donovan. Motoneurons regulate the central pattern generator during drug-induced locomotor-like activity in the neonatal mouse. *Elife*, 6:e26622, 2017.
82. Greg J Stanisz. Diffusion mr in biological systems: tissue compartments and exchange. *Israel journal of chemistry*, 43(1-2):33–44, 2003.
83. RD Dortch, RA Horch, and MD Does. Development, simulation, and validation of NMR relaxation-based exchange measurements. *The Journal of Chemical Physics*, 131(16): 164502, 2009.
84. Maxime Van Landeghem, Agnes Haber, Jean-Baptiste D'espinose De Lacaillerie, and Bernhard Blümich. Analysis of multisite 2d relaxation exchange nmr. *Concepts in Magnetic Resonance Part A*, 36(3):153–169, 2010.
85. Stefanie Eriksson, Karin Elbing, Olle Söderman, Karin Lindkvist-Petersson, Daniel Topgaard, and Samo Lasič. NMR quantification of diffusional exchange in cell suspensions with relaxation rate differences between intra and extracellular compartments. *PloS one*, 12 (5):e0177273, 2017.

Supporting Information Note 1: ADC provides a proxy for diffusion and DEXSY-derived volume fractions

Simultaneous realtime measurements were used to test for correlations between the metrics ADC_y, AXR, f (restricted water fraction), c, and f_{ng} (non-Gaussian signal fraction). ADC_y, f, and c arise from diffusion measurements. ADC_y measures the average mobility of all water molecules in the sample on the timescales of diffusion encoding (here between 0.20 and 0.51 ms). f and c are measured from fitting $I/I_0 = f\exp(-\tau c)$ to the MGSE signal attenuation at $b \geq 60\ \mathrm{ms}/\mu\mathrm{m}^2$ and are associated with localization or motional averaging of water near surfaces on the length scale of the gradient dephasing length ℓ_g (see Williamson, et al., Magn. Reson. Lett., 2023) Here, with the extremely strong $g = 15.3$ T/m static gradient produced by the low-field single-sided magnet, $\ell_g = 0.8\ \mu\mathrm{m}$ (at 25°C). c is the rate constant for the decay of this localized or motionally-averaged component as a function of SGSE echo time. c is related to a restriction length scale in the case of motional averaging, or D_0 in the case of localization, and also affected by exchange. ADC is a standard measurement used clinically (although with longer diffusion timescales between 20 and 100 ms), whereas f and c require gradient strengths not currently accessible with the pulsed gradients of clinical systems. f_{ng} is derived from the DEXSY data (see Eq. 19 in Cai, et al., J. Magn. Reson., 2024). Correlations between ADC and f have not been studied before, although they are often inferred in two-component models for ADC. Such models may include a hindered component and a restricted component with apparent diffusion coefficients D_1 and D_2 respectively, leading to $\mathrm{ADC} = (1-f)D_1 + fD_2$. Hindrances reduce D_1 below the diffusion coefficient of freely diffusing water, $D_0 = 2.15\ \mu\mathrm{m}^2/\mathrm{ms}$ at 25°C. Water that is restricted on length scales similar to or smaller than l_g will have $D_2 \ll D_1$, leading to $\mathrm{ADC} = (1-f)D_1$ in the limit that $D_2 = 0$. Note that the slope and intercept here are equal to D_1, the diffusion coefficient of the more mobile compartment. We use correlations to test this model and understand what the metrics are measuring in this system.

We find strong linear correlations between ADC_y and f (Figs. S1D and Figs. S5D). The correlation is the same regardless of the type of perturbation (with/without ouabain and osmolytes). Slopes and y-intercepts are similar to D_0 consistent with the model. These results are consistent with the picture that f is associated with effectively immobile water and ADC_y is a proxy for f. This suggests that both ADC_y and f report cellular swelling and shrinking.

ADC_y and f_{ng} are strongly correlated under normal conditions, with slope and intercept slightly above D_0, but not correlated after ouabain treatment (Figs. S1F). During osmolyte perturbations, the correlation appears strongest when $\Delta\mathrm{ADC}_y$ and Δf_{ng} are compared (Figs. S5F). The slopes are very close to 1, as predicted by the simple model. Deviations here are expected, since ADC_y and f are global measures averaged over the entire sample, whereas f_{ng} is a local measure averaged over exchanging compartments.

Supporting Information Note 2: Derivation of EEC-based model to predict tonicity

In this section we derive a model relating k to tonicity. The model is based on an application of transition state theory to the dynamics of mixtures. We first define the the enhancement of exchange with tonicity relative to a state of minimum (hypo)tonicity as $\theta = k_t/k_0$. Within transition state theory, $\theta = \exp(-\delta G_t/RT)$ where $\delta G_t = |G_t - G_0|$ is the change in Gibbs free energy associated with the difference in osmolarity of impermeable solutes in the extracellular space which increase the tonicity (hence the subscript t). Changes in Gibbs free energy can be decomposed into enthalpic and entropic contributions by its thermodynamic definition $\delta G_t = \delta E_{at} - T\delta S_t$. Then

$$\begin{aligned}\theta &= \exp\left(\frac{-(\delta E_{at} - T\delta S_t)}{RT}\right)\\ &= \exp\left(\frac{\delta S_t}{R} - \frac{-\delta E_{at}}{RT}\right)\\ &= \exp\left(\frac{\delta S_t}{R}\right)\exp\left(\frac{-\delta E_{at}}{RT}\right).\end{aligned} \tag{S1}$$

To become the Arrhenius model, we explicitly define the connections between the change in entropy and the preexponential factors $\exp(\delta S_t/R) = A_t/A_0$, and between the change in enthalpy and the activation energies $\delta E_{at} = E_{at} - E_{a0}$. Here, A_t and E_{at} are tonicity-dependent and A_0 and E_{a0} are evaluated when the system is at a a state of minimum (hypo)tonicity, defining $c = 0$. Then

$$\begin{aligned}\theta &= \frac{A_t}{A_0}\exp\left(\frac{-(E_{at} - E_{A0})}{RT}\right)\\ &= \frac{A_t}{A_0}\frac{\exp(-E_{at}/RT)}{\exp(-E_{a0}/RT)}\end{aligned} \tag{S2}$$

Now the effect of tonicity on exchange can be considered in terms of its separate effect on δE_{at} and δS_t.
The analytical functions for δE_{at} and δS_t with respect to the osmotic concentration can be obtained by Taylor expansions,

$$\begin{aligned} E_{at} &= E_{a0} + \left.\frac{dE_{at}}{dc}\right|_{\Delta c \to 0} \Delta c + O(\Delta c^2) + ... \\ S_t &= S_0 + \left.\frac{dS_t}{dc}\right|_{\Delta c \to 0} \Delta c + O(\Delta c^2) + ... \end{aligned} \tag{S3}$$

where $O(\Delta c^2) + ...$ refer to second- and higher-order terms and $|_{\Delta c \to 0}$ refers to the term being evaluated in the limit of $\Delta c \to 0$, i.e., $c_t \to c_0$. We limit ourselves to a first-order approximation so that a two-parameter model can be obtained, but with the downside that the model loses validity as Δc increases above dilute concentrations. We also drop the evaluated symbol for brevity (although still implied). Then

$$\begin{aligned} \delta E_{at} &\approx dE_{at}/dc\ \Delta c \\ \delta S_t &\approx dS_t/dc\ \Delta c. \end{aligned} \tag{S4}$$

These two parameters can be calculated from measurements of E_a and A at $c = c_0$ and c_1 with $\Delta c = c_1$ by using the relations $dE_{at}/dc = (E_{a(c=c_1)} - E_{a(c=c_0)})/\Delta c$ and $dS_t/dc = \ln(A_{c=c_1}/A_{c=c_0})R/\Delta c$. These are related to virial coefficients for the entropy and enthalpy of activation by $[E_{at}] = (dE_{at}/dc)/R$ and $[S_t] = (dS_t/dc)/R$. These definitions are combined with Eq. S1 to obtain the final relationship

$$\theta = \exp(-\alpha \Delta c) \tag{S5}$$

where

$$\begin{aligned} \alpha &= (\delta E_{at}/\Delta c RT) - (\delta S_t/\Delta c R) \\ &\approx (dE_{at}/dc)/RT - (dS_t/dc)/R \\ &\approx [E_{at}]/T - [S_t]. \end{aligned} \tag{S6}$$

From this model, it is also possible to calculate the tonicity Δc as

$$\Delta c = \ln(\theta)/\alpha. \tag{S7}$$

For our system, by comparing E_a and A of samples after treatment with ouabain to samples after treatment with ouabain and 100 mM sucrose ($c = c_0$ and $c = c_1$, respectively), we find $[E_{at}] = 16.1$ K/mM and $[S_t] = 0.0686$ 1/mM, leading to $\alpha \approx -0.0146$ 1/mM at 25°C. Based on k_t under normal and k_0 from ouabain-treated conditions $\theta = 130/35$, and Eq. S7 predicts $\Delta c = 90$ mOsm.

Supporting Information Note 3: Additional PLM and 3XM details

The pump–leak model (PLM) uses the finite difference method to approximate the fluxes of ions based on their governing differential equations for mass conservation. Na^+ and K^+ transport actively with a 3:2 stoichiometry. Na^+, K^+, and Cl^- transport passively based on their electrochemical potential. The net charge of the intracellular impermeants is $z = -1$. Water permeability is assumed to be much higher than ion permeability and is not modeled directly. Instead, the cell changes volume so that the intracellular osmolarity matches the extracellular osmolarity at the end of each timestep. Voltage is modeled based on the net charge of the intracellular ions and the (constant) capacitance of the membrane. Unless stated otherwise, simulation parameters were the same as in Kay (2017). Volumes and voltages were taken as the values obtained at the final timestep. This time was sufficiently long for systems to reach steady-state (if there existed a stable steady-state), as determined by volume and voltage not changing when total time was increased by a factor of 10.
An analytical equation for the steady-state ECS fraction (f_o) was developed based on an osmotic balance which includes the contribution of an uncharged, trapped ECS osmolyte (x_o);

$$f_o = 1 - \frac{(1-z)x_i}{w_{tot}(\pi - 2Cl_o \exp(FV/RT)) + x_o/f_o} \tag{S8}$$

where x_i is number of moles of intracellular impermeants, π is the concentration of small osmolytes in the ECS, Cl_o is the concentration of extracellular chloride, F is the Faraday constant, R is the ideal gas constant, and T is the absolute temperature. π and Cl_o are assumed equal to that of the bathing media. The ECS and ICS volumes sum to a fixed total volume, w_{tot}. While this model does not explicitly account for non-osmotic (e.g. hydrostatic and mechanical) pressure gradients which could become large when cells swell and push against one-another or when cells shrink and push on intracellular organelles, the trapped ECS

and ICS impermeant parameters act as placeholders to effectively model this buildup of pressure in cases of extreme swelling or shrinking. This equation does not model ion flux and instead assumes a value for the voltage (V). We used -48 mV for normal conditions and -10 mV for the conditions modeling $\mathrm{Na}^+/\mathrm{K}^+$–ATPase inhibition with ouabain. First, the PLM was used to find the steady-state cell volume predicted under normal conditions. This, along with $f_o = 0.3$ defined w_{tot}. Then x_o was arbitrarily set to $1/50$th of the moles of intracellular impermeants x_i. Then Eq. S8 was used to predict ECS fraction f_o and osmolarities of intracellular and extracellular impermeants at varying osmolarities for the $V = -48$ mV and -10 mV conditions.

A three-site exchange model (3XM) associated with an ECS compartment (**a**) and two ICS compartments (**b** and **c**) was developed for predicting ADC and k. Eq. S8 was used to define the fraction of compartment **a** ($f_c = f_o$). For simplicity, the fractions of the two ICS compartments were set equal, $f_b = f_c = (1 - f_a)/2$. The ECS compartment and a more mobile ICS compartment were both given $\mathrm{ADC}_a = \mathrm{ADC}_b = 1\ \mu\mathrm{m}^2/\mathrm{ms}$. A less mobile ICS compartment was given $\mathrm{ADC}_c = 0.1\ \mathrm{ms}/\mu\mathrm{m}^2$. Varying ADC values of the compartments affected the overall ADC, the size of effects on ADC, and the correlation between ADC and k but did not affect the overall interpretations or the EEC relationship. ADC was modeled as the sum of the ADC values of each compartment multiplied by their volume fraction, $\mathrm{ADC} = f_a\mathrm{ADC}_a + f_b\mathrm{ADC}_b + f_c\mathrm{ADC}_c$. k was modeled by simulating data from the DEXSY experiment and then fitting the exchange model to the data. DEXSY signals were modeled using an operator formalism $\mathbf{S} = [1,1,1] * OD_2 * OE * OD_1 * \mathbf{S}_0$, ignoring relaxation. This involved multiplication of matrix exponentials which used the function $\mathrm{expm}()$ in MATLAB 2024a. The operators for the first and second diffusion encoding blocks were $OD_{1,2} = \mathrm{expm}(-b_{1,2}\mathbf{D})$ with $\mathbf{D} = [\mathrm{ADC}_a, \mathrm{ADC}_b, \mathrm{ADC}_c]' . * \mathrm{eye}(3)$, where $\mathrm{eye}(3)$ is a 3×3 identity matrix. Equilibrium magnetization was $\mathbf{S}_0 = [f_c, f_b, f_a]'$. The exchange operator was $OE = \mathrm{expm}(-t_m\mathbf{K})$ with exchange matrix

$$\mathbf{K} = \begin{bmatrix} (f_b + f_c)k_t & -f_a k_t & -f_a k_t \\ -f_b k_t & f_a k_t + f_c k_g & -f_b k_g \\ -f_c k_t & -f_c k_g & f_a k_t + f_b k_g \end{bmatrix} \tag{S9}$$

including transmembrane exchange (k_t) and geometric exchange (k_g) pathways. k_t and k_g values were determined by the Arrhenius model (Eq. 2) with $T = 298.15$ K or varied in the simulation, using $E_a = 52\ \mathrm{kJ/mol}$ and $\ln(A) = 26.62\ \mathrm{s}^{-1}$ for k_t and $E_a = 22\ \mathrm{kJ/mol}$ and $\ln(A) = 12.52\ \mathrm{s}^{-1}$ for k_g. These $\ln(A)$ values were defined for each E_a using Eq. 3 and the slope and intercept values presented in the caption of Fig. 7. Parameters (timings, gradient, b_1 and b_2 protocol, mixing times, etc.) were set based on values used experimentally. k values were estimated using the same analysis method described in the "NMR hardware, experimental protocol, and analysis methods" section.

Supporting figures

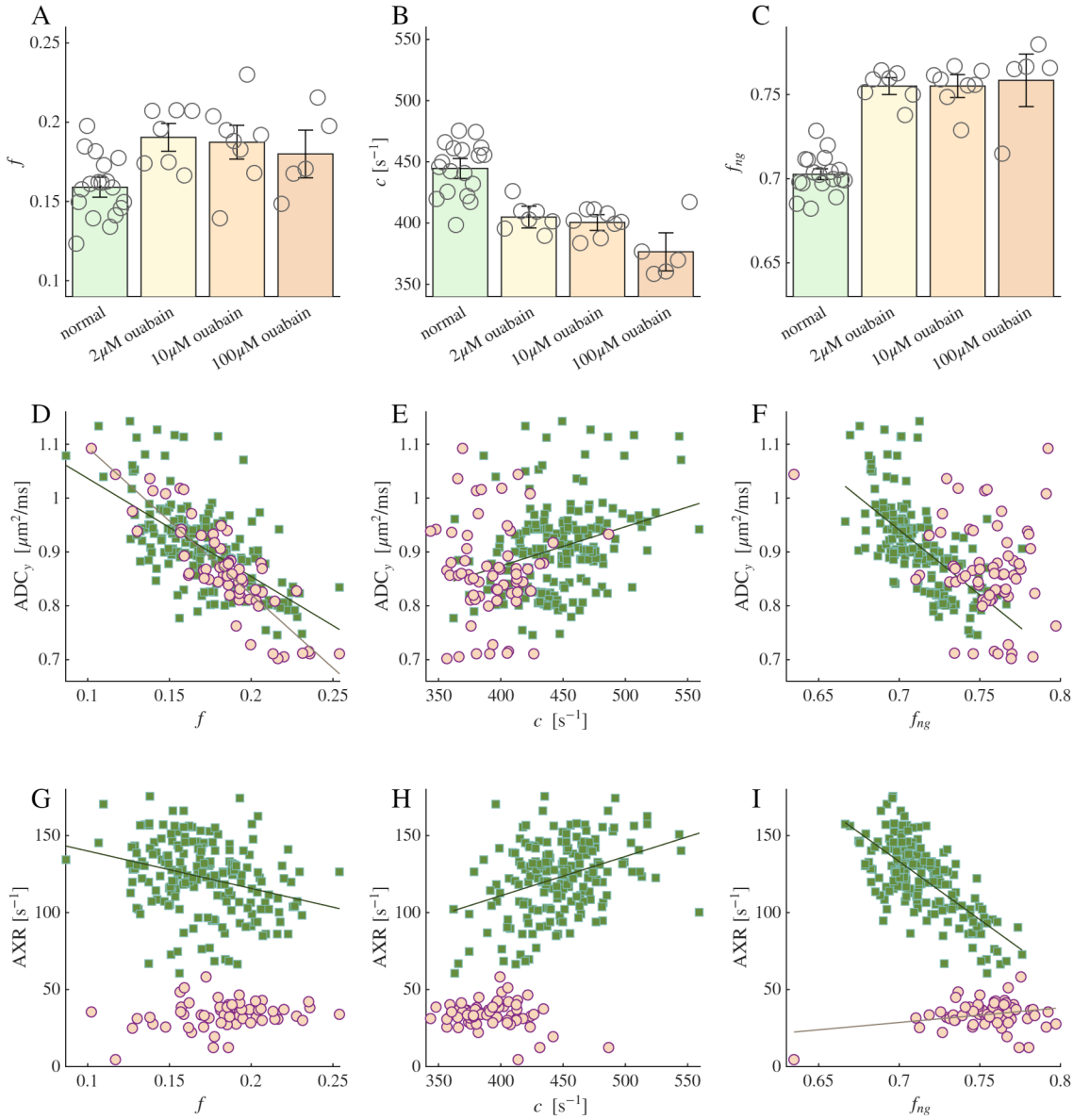

Fig. S1. Additional metrics and correlations from the effect of ouabain treatment A-C) Effect of ouabain on restricted fraction f and c from the intercept and slope of the SGSE diffusion signal at long times, and on the non-Gaussian signal fraction f_{ng} from the DEXSY data. D-I) Correlation of f, c, and f_{ng} vs. ADC_y and k. Data was grouped based on whether measurements occurred before (green squares) or after (pink circles) ouabain affected the exchange rate and dropped it below 60 s^{-1}. Linear fits are plotted when correlation is significant ($p < 0.05$). In (D), the data is significantly correlated for both groups ($p < 0.001$) with Pearson correlation coefficients (cc=) -0.64 before ouabain effect and cc=-0.87 after ouabain effect. Linear fits yielded $\mathrm{ADC}_y = -1.82f + 1.22\ \mu\mathrm{m}^2/\mathrm{ms}$ before ouabain effect and $\mathrm{ADC}_y = -2.72f + 1.36\mu\mathrm{m}^2/\mathrm{ms}$ after ouabain effect. In (F), the correlation is significant before the effect of ouabain, with ($p < 0.001$), cc=-0.65 and $\mathrm{ADC}_y = -2.4f_{ng} + 2.6\ \mu\mathrm{m}^2/\mathrm{ms}$, but is not significant after the effect.

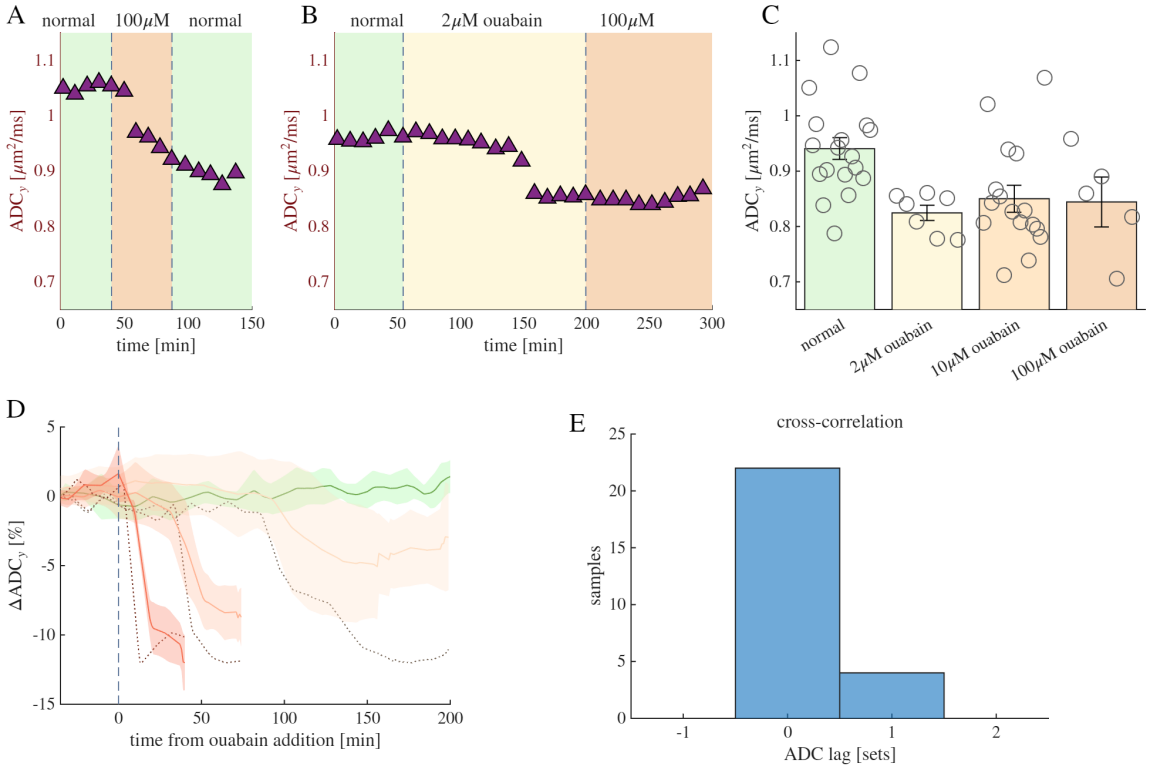

Fig. S2. ADC_y **and** k **are affected by ouabain simultaneously.** A–C) data reproduced from Fig. 1, but presenting the absolute values of ADC. Note the additional scatter between samples in (C) compared to when normalized by baseline values in Fig. 1C. D) Mean (solid lines) and standard deviation (shaded regions) of realtime ADC_y measurements from a control group under normal conditions (green) and groups treated with 2, 10, and 100 $\mu\mathrm{M}$ ouabain (lightest to darkest colors) plotted against the time after addition of ouabain. Dotted lines show the mean of k for each group, scaled to the maximum and minimum of the mean of ADC_y for comparison (refer to Fig. 1 for values) E) Histogram of the shift between the drop in ADC_y relative to the drop in k from a cross correlation analysis of 26 out of 28 samples for which there was a significant correlation between ADC_y and k ($cc > 0.2$, $p < 0.05$. Each set took 11 minutes to acquire and ADC_y measurements preceded k measurements. Analysis shows that ADC_y dropped either during the same set or the following set after k dropped, showing that ADC_y and k both dropped within 11 minutes of each other.

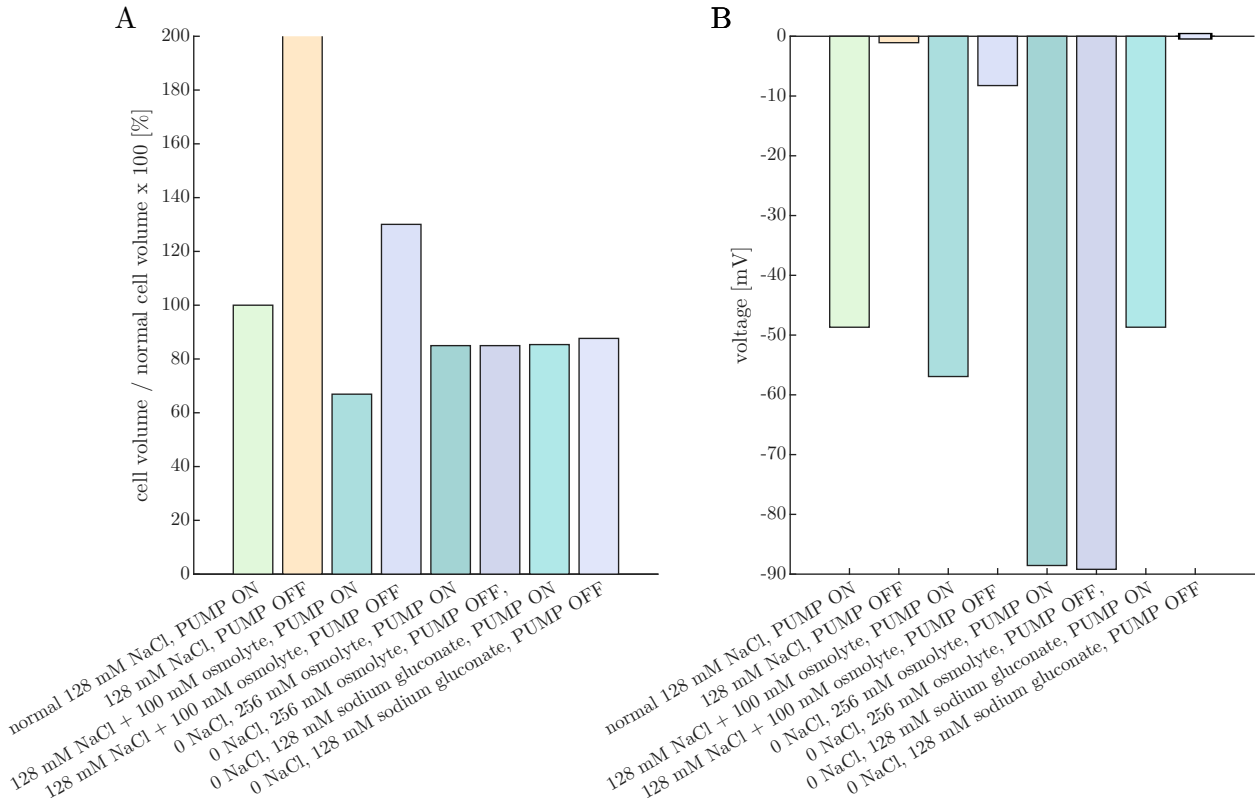

Fig. S3. Pump-leak model (PLM) provides predictions of cell volume and voltage under conditions studied experimentally. A) Percent change in cell volume and B) voltage predicted under various $\mathrm{Na}^+/\mathrm{K}^+$–ATPase PUMP ON or OFF and media conditions after the PLM has run to steady-state (if applicable). With the 128 mM NaCl (and 4 mM KCl) media and PUMP OFF condition, the cell continues to swell and does not reach a steady-state. Addition of an osmolyte (+100 mOsm) reduces the volume and hyperpolarizes the cell in the PUMP ON condition, and stabilizes the volume but does not recover the voltage with the PUMP OFF. The cell volume is reduced to a similar level in both the PUMP ON and PUMP OFF conditions when NaCl is replaced by either sucrose or sodium gluconate (modeled as uncharged and monovalent anionic impermeants in the bathing media, respectively). However, while voltage is similar between the PUMP ON and PUMP OFF conditions when NaCl is replaced by sucrose, full depolarization to $\mathrm{V} = 0$ is predicted in the PUMP OFF condition with NaCl replaced by sodium gluconate.

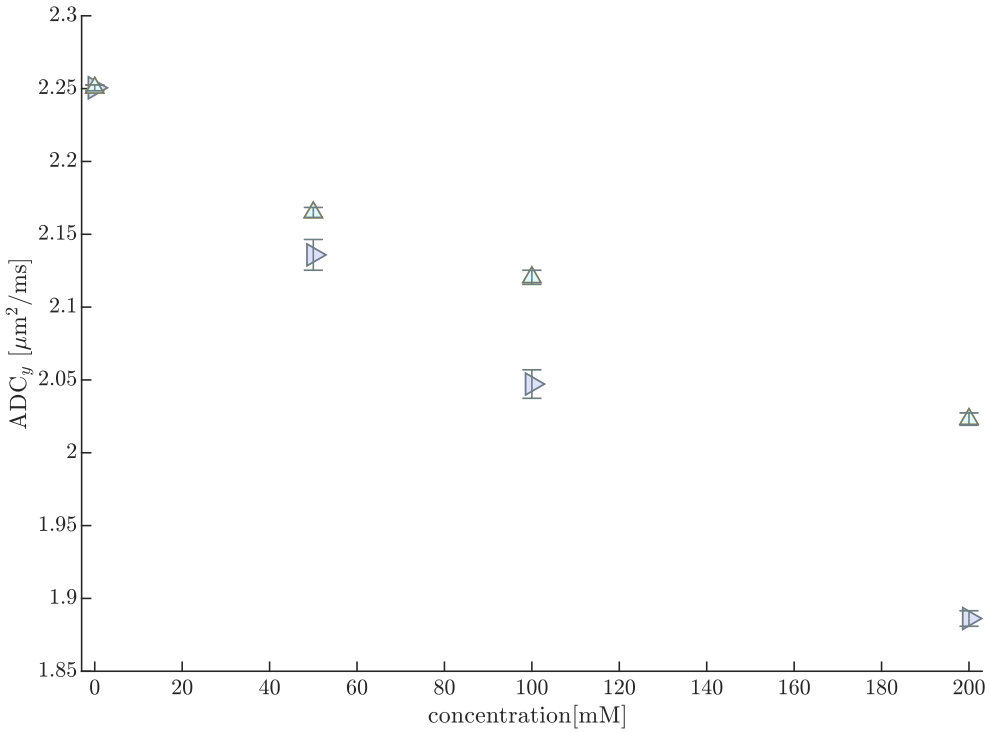

Fig. S4. Concentration-dependent effects of sucrose and mannitol on ADC of pure aCSF. Spin echo diffusion measurements were performed on aCSF at varying concentrations of sucrose (pink rightward-pointing triangles) or mannitol (aqua upward-pointing triangles) at 25°C without media circulation. At least three measurements were performed at each concentration using 8 τ values spaced linearly from $\tau = 105$ to $435\mu\mathrm{s}$ ($b = 0.0129$ to $0.9159\mathrm{ms}/\mu\mathrm{m}^2$), TR=2 s, and 2000 echoes. all other parameters were the same as standard diffusion measurements performed on spinal cords. Sucrose affects diffusion of water more than mannitol because it is a larger molecule (increased obstruction) and affects viscosity more (increased hydrodynamic interactions).

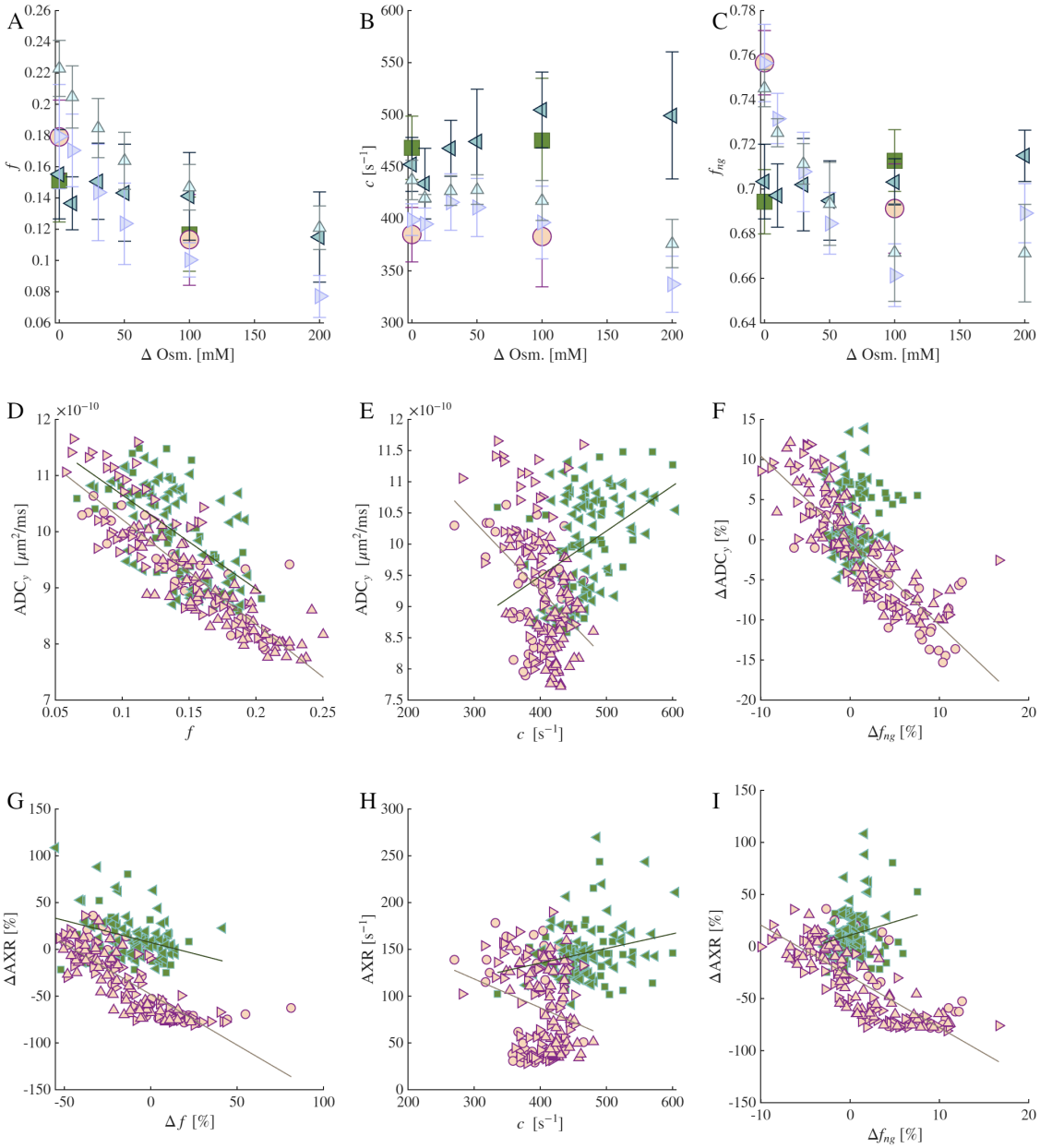

Fig. S5. Additional metrics and correlations from the effects of osmolytes without and with ouabain treatment A-C) Effect of osmolytes on f and c from the intercept and slope of the SGSE diffusion signal at long times, and on the non-Gaussian signal fraction f_{ng} from the DEXSY data. Refer to Fig. 1 for legend. D-I) Correlation of f, c, and f_{ng} vs. ADC_y and k. Data was normalized in cases where it tightened the correlation. In (D), cc= -0.61 without ouabain and cc=-0.87 with ouabain. Linear fits yielded $\mathrm{ADC}_y = -1.67f + 1.23\ \mu\mathrm{m}^2/\mathrm{ms}$ without ouabain and $\mathrm{ADC}_y = -1.87f + 1.21\mu\mathrm{m}^2/\mathrm{ms}$ with ouabain (note the slope slightly reduced from D_0). in (F), the correlation was insignificant without ouabain. With oabain, the correlation was significant ($p < 0.001$) with cc=-0.85 and linear fits yielded $\Delta\mathrm{ADC}_y = -1.05\Delta f_{ng} + 0.11\ \%$ (note the slope near 1). Note the sigmoidal correlations between Δf vs. $\Delta\mathrm{AXR}$ and Δf_{ng} vs. $\Delta\mathrm{AXR}$